CHEMISTRY
A EUROPEAN JOURNAL

DOI: 10.1002/chem.200700261

Ligand Reprogramming in Dinuclear Helicate Complexes: A Consequence of Allosteric or Electrostatic Effects?

John C. Jeffery,[a] Craig R. Rice,[b] Lindsay P. Harding,[b] Christian J. Baylies,[b] and Thomas Riis-Johannessen*[a, c]

Abstract: The ditopic ligand 6,6′-bis(4-methylthiazol-2-yl)-3,3′-([18]crown-6)-2,2′-bipyridine ($\mathbf{L^1}$) contains both a potentially tetradentate pyridyl-thiazole (py-tz) N-donor chain and an additional "external" crown ether binding site which spans the central 2,2′-bipyridine unit. In polar solvents (MeCN, $MeNO_2$) this ligand forms complexes with Zn^{II}, Cd^{II}, Hg^{II} and Cu^{I} ions via coordination of the N donors to the metal ion. Reaction with both Hg^{II} and Cu^{I} ions results in the self-assembly of dinuclear double-stranded helicate complexes. The ligands are partitioned by rotation about the central py–py bond, such that each can coordinate to both metals as a bis-bidentate donor ligand. With Zn^{II} ions a single-stranded mononuclear species is formed in which one ligand coordinates the metal ion in a planar tetradentate fashion. Reaction with Cd^{II} ions gives rise to an equilibrium between both the dinuclear double-stranded helicate and the mononuclear species. These complexes can further coordinate s-block metal cations *via* the remote crown ether O-donor domains; a consequence of which are some remarkable changes in the binding modes of the N-donor domains. Reaction of the Hg^{II}- or Cd^{II}-containing helicate with either Ba^{2+} or Sr^{2+} ions effectively reprogrammes the ligand to form only the single-stranded heterobinuclear complexes $[MM'(\mathbf{L^1})]^{4+}$ ($M = Hg^{II}$, Cd^{II}; $M' = Ba^{2+}$, Sr^{2+}), where the transition and s-block cations reside in the N- and O-donor sites, respectively. In contrast, the same ions have only a minor structural impact on the Zn^{II} species, which already exists as a single-stranded mononuclear complex. Similar reactions with the Cd^{II} system result in a shift in equilibrium towards the single-stranded species, the extent of which depends on the size and charge of the s-block cation in question. Reaction of the dicopper(I) double-stranded helicate with Ba^{2+} shows that the dinuclear structure still remains intact but the pitch length is significantly increased.

Keywords: allosterism · helical structures · ligand programming · N ligands · supramolecular chemistry

Introduction

There are now thousands of articles in the literature which testify to the value of multidentate ligands, capable of partitioning into different binding domains, in the design and self-assembly of metallosupramolecular complexes.[1] It has also been well established that the structural topology of a given assembly is strongly influenced, indeed fully governed in some cases, by the nature, number and disposition of the binding sites within the ligand strand. Judicious consideration of these factors has thus enabled the isolation and characterisation of a myriad of elaborate structures featuring helical,[1e–h] grid,[1i–k] cylindrical,[1l–m] and cage[1n–o] topologies. Once a ligand has been synthesised, however, this geometric information is permanently stored within it and the ligand can therefore be considered as being *pre-programmed*.

We have recently demonstrated how the intrinsic information stored within a ligand strand can be modified or reprogrammed by introducing s-block cations into a remote crown ether binding site tethered to the periphery of the ligand. For example, the ditopic ligand $\mathbf{L^1}$ (see below), which assembles into a dinuclear double-stranded helicate on combina-

[a] Dr. J. C. Jeffery, Dr. T. Riis-Johannessen
The School of Chemistry, University of Bristol
Bristol BS81TS (UK)
E-mail: thomas.riis@chiam.unige.ch

[b] Dr. C. R. Rice, Dr. L. P. Harding, Dr. C. J. Baylies
Department of Chemical and Biological Sciences
University of Huddersfield, Huddersfield HD13DH (UK)

[c] Dr. T. Riis-Johannessen
Current address:
Section de Chimie et Biochimie, Université de Genève
Sciences II, 30, quai Ernest-Ansermet
1211 Genève 4 (Switzerland)
Fax: (+41)22-379-6023

tion with Hg^{II}, may be reprogrammed to bind one Hg^{II} ion in a tetradentate fashion following the addition of Ba^{2+} or Sr^{2+} ions.[2] In binding to the crown ether macrocycles, the s-block cations essentially render the ligand unsuitable for sustaining the helicate assembly in the presence of Hg^{II} ions. Furthermore, the same ligand's preference for different metal ions[3] and the pitch-length of helicate complexes of a related ligand $\mathbf{L^2}$ (see above)[4] have been modified by similar approaches.

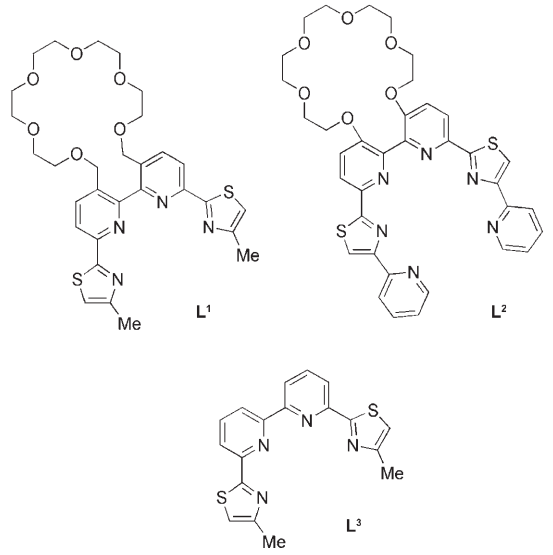

In this paper we present the results of a detailed investigation into the complexes of $\mathbf{L^1}$ with all three Group XII dications and the Group XI monocation Cu^{I}, in which their behaviour both in the presence and absence of various s-block cations is assessed. Systematic variation of charge and ionic radius on the transition-metal cation gives insight into some of the factors which contribute to the structural changes induced when different s-block cations are introduced into the crown ether macrocycle. The observed responses have then been compared qualitatively and possible conclusions regarding the origins of the ligand reprogramming effect are drawn. We note, however, that some of the structural and spectroscopic data described herein have been published previously. The mercury-containing crystal structures **3** and **5** and ^{1}H NMR titrations of these complexes with s-block cations Na^+ and Ba^{2+} appeared in a preliminary communication, detailing how the ligand's Hg^{II}-binding modes could be modified by complexation of s-block cations.[2] Likewise, the zinc(II) and copper(I) structures **1** and **7** featured in a later communication which focused on the use of s-block cation binding for tuning the selectivity of the ligand $\mathbf{L^1}$ for different transition-metal cations.[3]

Results and Discussion

Ligand synthesis: The synthesis of ligands $\mathbf{L^1}$ is outlined in Scheme 1. The 3,3′-dimethylol-2,2′-bipyridine precursor was prepared in high yield from 1,10-phenanthroline following procedures described by Shan et al. and Rebek et al.[20] Reaction of the dimethylol with penta(ethylene glycol)-di-*p*-toluenesulfonate using sodium hydride as a deprotonating agent, then afforded the bipyridyl crown ethers in mediocre yields of 40–50%.

The terminal 4-methylthiazol-2-yl arms were appended following an adapted version of the procedure described by Baxter et al. for the monotopic ligand $\mathbf{L^3}$.[9] The bipyridyl crown ether 3,3′-([12]-crown-4)-2,2′-bipyridine was converted into the bis-*N*,*N*′-oxide using *meta*-chloroperoxybenzoic acid. Refluxing a dichloromethane solution of the latter with excess trimethylsilyl cyanide in the presence of benzoyl chloride then afforded the dicyano derivatives in high yield. The remaining steps were carried out as for $\mathbf{L^3}$, although the final ligand and all intermediates required purification by column chromatography. Slow evaporation of an acetonitrile solution of $\mathbf{L^1}$ afforded colourless microcrystals allowing solid-state structural confirmation by X-ray crystallography (see Experimental Section, CCDC-637061).

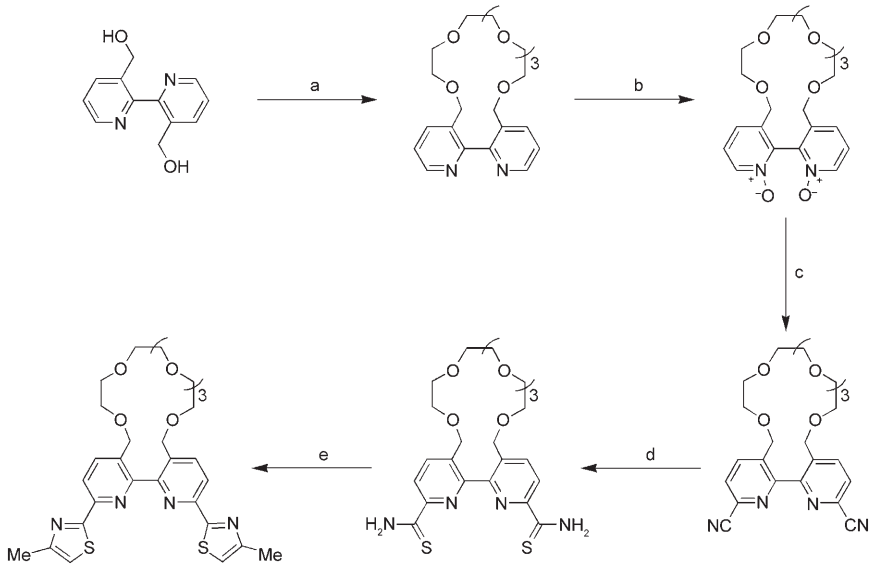

Scheme 1. a) Penta(ethylene-glycol) di-*p*-toluenesulfonate, DMF, NaH; b) *m*CPBA, CH_2Cl_2; c) TMSCN, PhCOCl, CH_2Cl_2; d) H_2S, Et_3N, EtOH; e) chloroacetone, EtOH.

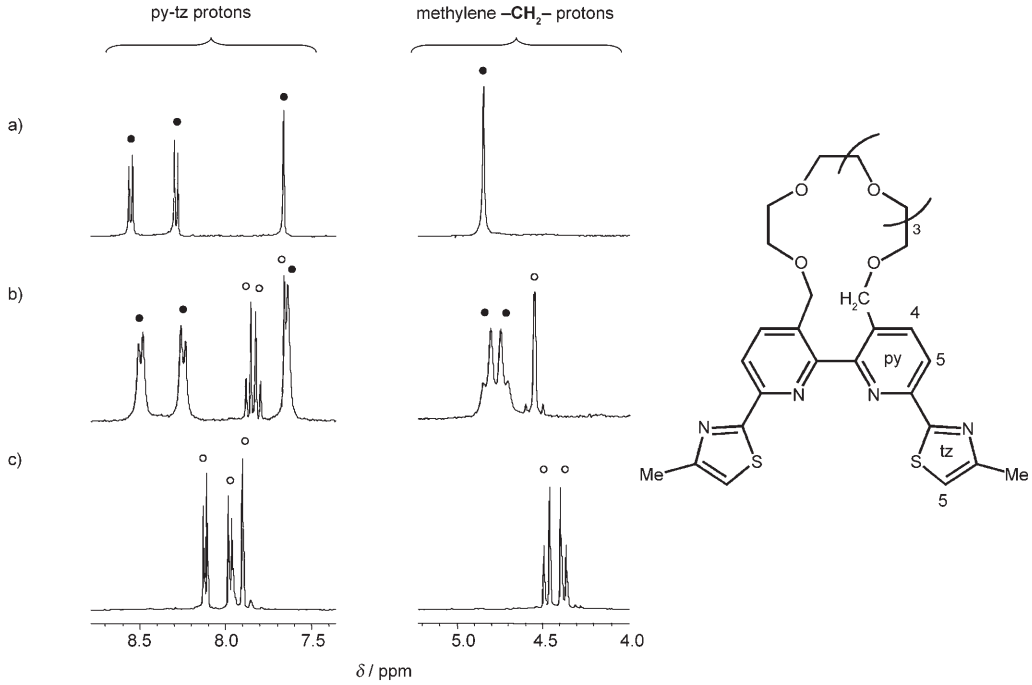

Figure 1. Selected regions of the ^{1}H NMR spectra of solutions (CD_3CN) containing equimolar amounts of $\mathbf{L^1}$ and a) $[Zn(H_2O)_6][ClO_4]_2$, b) $[Cd(H_2O)_6][ClO_4]_2$ and c) $[Hg(H_2O)_3][ClO_4]_2$. The symbols denote peaks assigned to single-stranded mononuclear $[M(\mathbf{L^1})]^{2+}$ (●) and double-stranded dinuclear $[M_2(\mathbf{L^1})_2]^{4+}$ (○) species. The inset picture shows the proton numbering scheme.

Complexes of $\mathbf{L^1}$ with zinc(II), cadmium(II) and mercury(II): Complexes of $\mathbf{L^1}$ with zinc(II), cadmium(II) and mercury(II) were prepared by combining equimolar amounts of ligand with an appropriate metal salt $[M(H_2O)_6][ClO_4]_2$ (M = Zn^{II}, Cd^{II} or Hg^{II}) in acetonitrile. Attempts to isolate crystalline materials were unsuccessful and solid-state characterisation (crystallography, elemental analysis) was thus precluded; however, the electrospray ionisation mass spectra for solutions (MeCN) prepared in situ were informative. In each case, large peaks corresponding to mononuclear complexes $[M(\mathbf{L^1})(ClO_4)_n]^{(2-n)+}$ (M = Zn^{II}, Cd^{II} or Hg^{II} and $n = 0$ or 1) were observed. The spectra also provided evidence for higher mass species with peaks at m/z 1389.3, 1653.2 (for Zn^{II}); 1437.5, 1747.1 (for Cd^{II}); and 1525.3, 1925.2 (for Hg^{II}) corresponding to mono- and dinuclear complexes of the type $[M(\mathbf{L^1})_2(ClO_4)_n]^{(2-n)+}$ (M = Zn^{II}, Cd^{II} or Hg^{II}; $n = 0$, 1) and $[M_2(\mathbf{L^1})_2(ClO_4)_3]^+$ (M = Zn^{II}, Cd^{II} or Hg^{II}), respectively. The relative peak intensities suggest that these species (in particular the dinuclear complex) are present in the gas-phase in significant quantities (> 10%) only when M = Hg^{II}. As the Group XII is ascended signals corresponding to dinuclear species are incrementally reduced in intensity.

^{1}H NMR Spectroscopy: Solutions (CD_3CN, $[\mathbf{L^1}]_{tot} = 0.04$ M) containing an equimolar M/$\mathbf{L^1}$ mixture (M = Zn^{II}, Cd^{II}, Hg^{II}) were examined by 400 MHz ^{1}H NMR spectroscopy. The aromatic and methylene regions are shown in Figure 1; the chemical shift data are summarised in Table 1. For both M = Zn^{II} and Hg^{II} a total of three pyridyl-thiazole (py-tz) ^{1}H signals appear in the aromatic region, consistent with the formation of either single- or double-stranded complexes which

Table 1. Chemical shifts (δ) of selected ^{1}H resonances observed in the NMR spectra of a) $\mathbf{L^1}$ and its complexes with Group XII dications and, for comparison, b) helicate and mononuclear complexes of $\mathbf{L^2}$.

	py-H(3)	py-H(4)	py-H(5)	tz-H(5)	-CH_3	Solvent	Ref.
complexes of $\mathbf{L^1}$							
$\mathbf{L^1}$	–	8.13	8.18	7.15	2.49	CD_3CN	–
$[Zn(\mathbf{L^1})]^{2+}$[a]	–	8.55	8.28	7.66	2.78	CD_3CN	–
$[Cd(\mathbf{L^1})]^{2+}$[a]	–	8.50	8.26	7.65	2.73	CD_3CN	–
$[Cd_2(\mathbf{L^1})_2]^{4+}$[b]	–	7.88	7.82	7.66	2.50	CD_3CN	–
$[Hg_2(\mathbf{L^1})_2]^{4+}$[b]	–	7.97	8.12	7.90	2.61	CD_3CN	–
$[Cu_2(\mathbf{L^1})_2]^{2+}$[b]	–	7.64	7.79	7.53	2.31	CD_3CN	–
complexes of $\mathbf{L^2}$							
$[Zn(\mathbf{L^2})]^{2+}$[c]	8.76	8.55	8.45	7.85	2.85	CD_3OD	[9]
$[Cd(\mathbf{L^2})]^{2+}$[c]	8.82	8.55	8.49	7.92	2.86	CD_3OD	[5]
$[Hg(\mathbf{L^2})]^{2+}$[c]	8.73	8.54	8.42	7.87	2.98	CD_3NO_2	[5]
$[Cu2(\mathbf{L^2})2]^{2+}$[c]	8.00	8.10	7.88	7.31	1.90	CD_3NO_2	[5]
$[Ag2(\mathbf{L^2})2]^{2+}$[c]	8.10	8.16	7.94	7.24	1.71	CD_3CN	[5]

[a] Tentative assignment of pyridyl protons py-H(4)/(5). [b] Py-H(4)/(5) assignment based on NOESY spectra. [c] Tentative assignment of pyridyl protons py-H(3)/(5).

achieve respective C_2- or D_2-symmetries on the NMR timescale. When $M=Zn^{II}$ (Figure 1a) the py-tz ^1H chemical shifts fall within the characteristic range (ca. $8.4 < \delta < 8.9$) for previously characterised single-stranded mononuclear complexes $[M(\mathbf{L^2})]^{2+}$ ($M=Zn^{II}$, Cd^{II}, Hg^{II}).[5] When $M=Hg^{II}$ (Figure 1c) the same protons appear upfield and fall within the characteristic shift range (ca. $7.2 < \delta < 8.2$) for previously characterised double-stranded helicate complexes $[M_2(\mathbf{L^2})_2]^{2+}$ ($M=Cu^{I}$, Ag^{I}).[5] That py protons H(4) and H(5) appear upfield (in the Hg^{II} complex) with respect to the free ligand is strongly indicative of helical wrapping of two or more ligand strands; this subjects protons on one ligand to shielding ring currents caused by the aromatic heterocycles in the other ligand (and vice versa). When $M=Cd^{II}$ the spectrum shows two major sets of peaks consistent with the presence of both (single- and double-stranded) species.

These assignments are easily reconciled with the mass spectra, which showed an increasing abundance of dinuclear double-stranded species on descending the Group XII dications. Assignment of the solutions structures in the cadmium(II) system is further supported by the $^1H,^1H$ NOESY spectrum (Figure 2). NOE signals between the $-CH_2-$ and Me protons are only observed for the proposed helicate complex $[Cd_2(\mathbf{L^1})_2]^{4+}$, wherein the $-CH_2-$ protons on one ligand strand are brought into close proximity to the Me protons on the other strand. In the single-stranded mononuclear complex (or the free ligand) the distance between these sites is too great for through-space or through-bond interactions to be observed. The NOESY spectrum also contains off-diagonal peaks corresponding to exchange between the same protons on different species (helicate vs mononuclear). These are most apparent for the py protons $H(4)_{hel}$/$H(4)_{mon}$ and $H(5)_{hel}$/$H(5)_{mon}$ (Figure 2).

Variable temperature studies: The ^1H NMR spectra of solutions (CD_3CN, $[\mathbf{L^1}]_{tot}=0.04$ M) containing equimolar M/$\mathbf{L^1}$ ($M=Zn^{II}$, Cd^{II}, Hg^{II}) were studied over the temperature range $233 \le T \le 343$ K allowing the following intra- and intermolecular exchange processes to be monitored: i) racemisation of the methylene $-CH_2-$ protons in both mononuclear complexes $[M(\mathbf{L^1})]^{2+}$ ($M=Zn^{II}$ and Cd^{II}) and ii) changes in the position of the $[Cd_2(\mathbf{L^1})_2]^{4+} \rightleftarrows 2[Cd(\mathbf{L^1})]^{2+}$ equilibrium.

Rates of racemisation (k_c) at coalescence temperature (T_c) for the methylene protons in mononuclear complexes $[M(\mathbf{L^1})]^{2+}$ ($M=Zn^{II}$ and Cd^{II}) were estimated using a simple analysis of $\Delta\nu$—the difference in frequency (Hz) between the two signals in the absence of exchange—and the scalar coupling constant (J).[6] Gibbs free energies of activation $\Delta G^{\ddagger}_{rac}$ for racemisation were then obtained using the Eyring equation; values of $\Delta G^{\ddagger}_{rac} = +53$ and $+66$ ($\pm \approx 2$) kJ mol^{-1} were calculated for $[Zn(\mathbf{L^1})]^{2+}$ and $[Cd(\mathbf{L^1})]^{2+}$, respectively. Coalescence (or even broadening) of the methylene protons in the $[M_2(\mathbf{L^1})_2]^{4+}$ ($M=Cd^{II}$, Hg^{II}) helicates was not observed within the solvent accessible temperature range.

$$k_c = \frac{\pi\sqrt{\Delta\nu^2 + 6J^2}}{\sqrt{2}}$$

For the mononuclear $[M(\mathbf{L^1})]^{2+}$ ($M=Zn^{II}$ and Cd^{II}) complexes, the increase in $\Delta G^{\ddagger}_{rac}$ observed on replacing Zn^{II} with Cd^{II} is significant and implies close interplay or cooperativi-

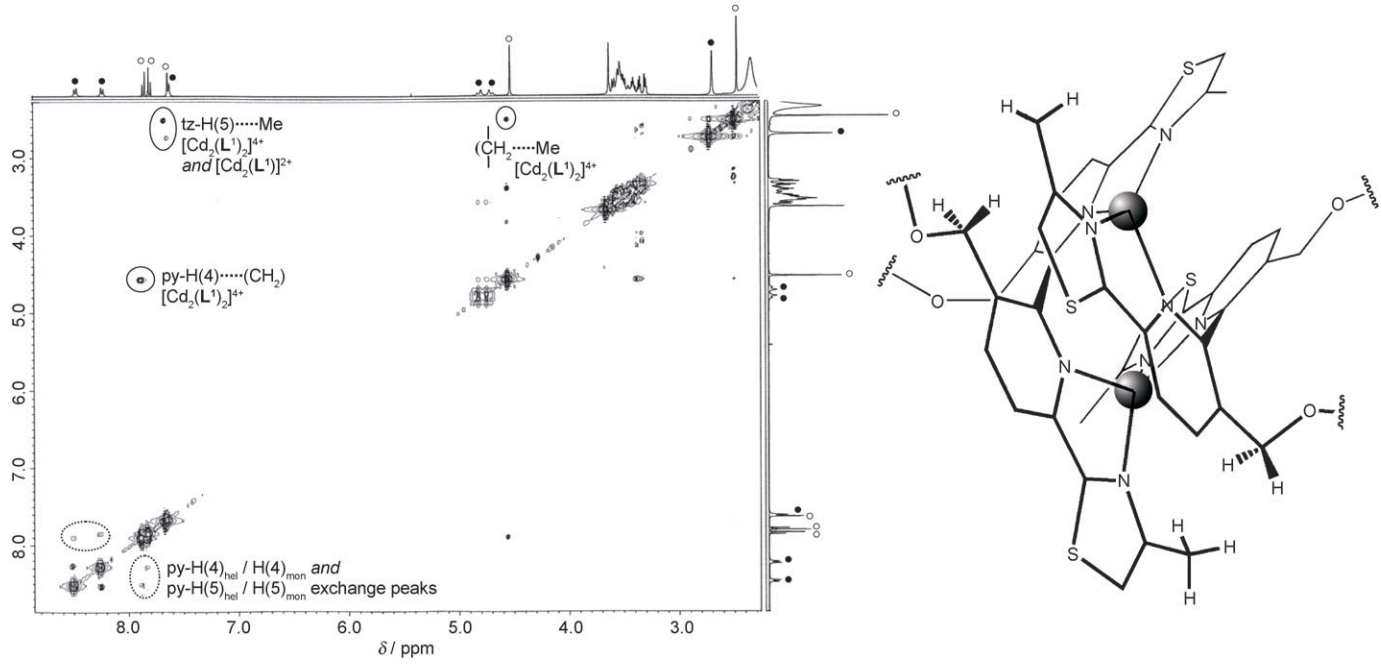

Figure 2. $^1H,^1H$ NOESY spectrum of a solution (CD_3CN) containing equimolar $[Cd(H_2O)_6][ClO_4]_2$ and $\mathbf{L^1}$. Off-diagonal peaks corresponding to NOEs are circled with a solid line (——), whilst those which correspond to exchange peaks are circled with a dotted line (·····). The symbols denote single-stranded mononuclear $[Cd(\mathbf{L^1})]^{2+}$ (●) and double-stranded dinuclear $[Cd_2(\mathbf{L^1})_2]^{4+}$ (○) species.

ty between the transition-metal binding (py-tz) domains and the crown ether macrocycle. Providing that racemisation is i) mechanically coupled to and ii) requires considerable movement or possibly even dissociation of (at least one of) the coordinating py-tz arms, it is likely that the observed change in $\Delta G^{\neq}_{rac}$ reflects how strongly each metal ion interacts with the py-tz N donors. Essentially, a stronger set of M–N bonds would restrain the necessary movement in the py-tz arms for rapid racemisation of the methylene protons to occur, and by implication greater stability is expected for the complex with the higher $\Delta G^{\neq}_{rac}$, that is, $[Cd(\mathbf{L^1})]^{2+}$. This speculation is in accord with detailed studies previously carried out by Williams and co-workers into the correlation between lability and stability in a series of dicopper(I) helicates.[7] In the case of the double-stranded helicates (Figure 1b and c), smaller values of $\Delta\nu$ and arguably sharper resonances for the methylene protons (cf. the single-stranded mononuclear cadmium(II) and zinc(II) complexes) indicate a further increase in the energy barrier $\Delta G^{\neq}_{rac}$ for racemisation. This is not alarming given that the racemisation mechanism will now be a two-step process and require at least twice as many M–N bond disturbances for inversion to occur.

Equilibrium constants K_{eq} for the $[Cd_2(\mathbf{L^1})_2]^{4+} \rightleftarrows 2[Cd(\mathbf{L^1})]^{2+}$ equilibrium were also calculated for a selection of temperatures over the range $298 \leq T \leq 343$ K. The corresponding plot of $\ln K_{eq}$ versus $1/T$ was linear ($R^2 = 0.99$) and values of $\Delta_r H = 47$ (± ca. 1) kJ mol^{-1} and $\Delta_r S = 131$ (± ca. 2) J mol^{-1} K^{-1} were estimated for the forward fragmentation process. Interestingly, when carried out on spectra recorded in deuterated nitromethane (CD_3NO_2) the same analysis afforded values of $\Delta_r H = 55$ (± ca. 1) kJ mol^{-1} and $\Delta_r S = 162$ (± ca. 2) J mol^{-1} K^{-1}. Although a slight enthalpic shift in favour of the more highly charged helicate complex is anticipated on increasing solvent polarity (solvent dielectric constants are 37.5 for CD_3CN and 39.4 for CD_3NO_2), a shift of this magnitude tends to implicate other factors. Indeed, the respective solvent donor abilities may also strongly influence the equilibrium. As suggested by the frequent detection of MeCN-substituted adducts $[M(\mathbf{L^3})(MeCN)_n]^{2+}$ (M = Co^{II}, Ni^{II}, Cu^{II}, Cd^{II}, Hg^{II} etc.; $n = 1$, 2) when characterising the (previously reported) complexes of $\mathbf{L^3}$ (see above) in the gas-phase,[5] mononuclear complexes of this kind clearly benefit from coordination of a donor solvent to the axial sites on the metal. Accordingly, one possibility for the observed shift in $\Delta_r H$ is that the mononuclear complex $[Cd(\mathbf{L^1})]^{2+}$ becomes more destabilised (with respect to the helicate) on replacing CD_3CN with CD_3NO_2 due to the limited capacity of nitromethane to coordinate the axial positions of the metal in former complex. Again, similar solvent effects were observed in the series of dicopper(I) helicates previously investigated by Williams and co-workers.[7]

Although analysis of the temperature dependence of K_{eq} for the zinc(II) and mercury(II) systems was precluded due to insufficient variation of the mononuclear/helicate signal intensities over the solvent accessible temperature ranges, it is possible to speculate on the relative stabilities of each complex type for all Group XII dications. Assuming that i) there is marginal variation of $\Delta_r S$ for the $[M_2(\mathbf{L^1})_2]^{4+} \rightleftarrows 2M(\mathbf{L^1})]^{2+}$ reaction on descending the Group XII dications and ii) $\Delta_r S$ remains relatively large and positive for the forward process, the dramatic change in K_{eq} on descending the Group XII cations may be primarily attributed to enthalpic contributions $\Delta_r H$. When M = Hg^{II} a more positive $\Delta_r H$ (relative to the Cd^{II} system) strongly favours the double-stranded helicate, whereas when M = Zn^{II}, $\Delta_r H$ is reduced (relative to the Cd^{II} system) and the single-stranded complex prevails within the solvent accessible temperature range.

The Group XII dications have closed-shell d^{10} electronic configurations and thus lacking concrete stereochemical arguments, a possible explanation for this trend requires consideration of the respective ionic radii r. From Table 2 it is evident that the preference for helicate formation and ionic radius r are closely correlated; as r increases, so too does the apparent relative stability of the helicate species. Whilst the ionic radius r for a given metal dication may not have an overwhelming influence on the degree of N-donor stabilisation achieved in either complex type (helicate vs mononuclear), it will affect electrostatic repulsion within the dinuclear helicate. In the latter, not only will the ionic radius determine the M–N separations, they will also determine how far apart the metals are situated within the helicate. Smaller ions will require shorter M–N separations and, in particular, optimising the M–N$_{(py)}$ bond lengths brings the two metals into close proximity with one another. The resulting electrostatic repulsion may thus dramatically reduce $\Delta_r H$ for systems based on smaller ions, such as zinc(II), with respect to the larger ions Cd^{II} and Hg^{II}. Further encouraged by a favourable entropy term for the helicate disassembly, as r decreases the smaller dications are brought into such close proximity that the strained mononuclear complex becomes energetically more favourable.

Table 2. Ionic radii r of the Group XII dications.

	$[M(\mathbf{L^1})]^{2+}/[M_2(\mathbf{L^1})_2]^{4+}$ ratio (at RT)	Ionic radius (r)/Å[a]
zinc(II)	ca. 99:1	$0.60 \leq r \leq 0.74$
cadmium(II)	ca. 70:30	$0.78 \leq r \leq 0.95$
mercury(II)	ca. 1:99	$0.96 \leq r \leq 1.02$

[a] The ranges describe Shannon radii for four-, five- and six-coordinate ions.[8]

Complex of $\mathbf{L^1}$ with copper(I): The copper(I) complex of $\mathbf{L^1}$ was prepared by reacting equimolar amounts of ligand with $[Cu(MeCN)_4][PF_6]$ in acetonitrile. Attempts at isolating a pure crystalline material were again unsuccessful, but the electrospray ionisation mass spectra for solutions prepared in situ showed intense peaks corresponding to the double-stranded dinuclear species.

^{1}H NMR Spectroscopy: As for the dimercury(II) complex $[Hg_2(\mathbf{L^1})_2]^{4+}$ (Figure 1c), the 400 MHz ^{1}H NMR spectrum of $[Cu_2(\mathbf{L^1})_2]^{2+}$ (CD_3CN, $[\mathbf{L^1}]_{tot} = 0.04$ M) shows three signals in the aromatic region, two diastereotopic methylene signals in

the aliphatic region and signals for the terminal Me and crown ether substituents. The chemical shifts (Table 1) are typical of di(mono)cationic double-stranded complexes of tetradentate py-tz ligands,[5] whilst the total number of observed peaks is consistent with the formation of a solution-phase helicate structure which achieves D_2 symmetry on the NMR timescale.

s Block cation binding studies

Zinc(II) system: The ^{1}H NMR spectrum of a solution (CD_3CN, $[\mathbf{L^1}]_{tot} = 0.04$ M) containing equimolar $[Zn(H_2O)_6][ClO_4]_2$ and $\mathbf{L^1}$ was recorded before and after treatment with one equivalent of $Ba(ClO_4)_2$ (Figure 3). Comparison of the

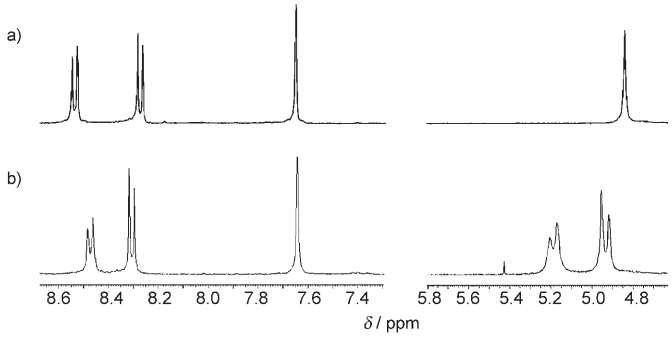

Figure 3. Selected regions of the ^{1}H NMR spectrum of a) a solution (CD_3CN) containing equimolar $\mathbf{L^1}$ and $[Zn(H_2O)_6][ClO_4]_2$ and b) the same solution after the addition of one equivalent of $Ba(ClO_4)_2$ or $Sr(ClO_4)_2$.

spectra shows that whilst the aromatic region remains largely unaffected, the methylene protons ($4.6 < \delta < 5.4$) experience a significant change in both chemical shift and dynamic behaviour following addition of Ba^{2+} ions; the initial singlet resonance being resolved into two doublets, both of which are shifted downfield by up to 0.4 ppm.

The dramatic changes in chemical shift $\Delta\delta$ for the methylene protons indicate uptake of Ba^{2+} ions by the [18]crown-6 macrocycle in $\mathbf{L^1}$; both protons are deshielded due to their proximity to the Lewis acidic Ba^{2+} ion. Resolution of the initial singlet into two doublets can be ascribed to the restricted conformational mobility induced by coordination of a Ba^{2+} ion to the crown ether host cavity. However, that relatively minor changes occur in the aromatic region ($\Delta\delta_{max} \approx 0.1$) is consistent with the retention of a similar single-stranded zinc(II) complex to that formed in the absence of Ba^{2+} ions. Treatment with $Sr(ClO_4)_2$ or $K(ClO_4)$ had similar consequences; in each case a significant downfield shift was observed for only the methylene protons.

These results were supported by an X-ray crystallographic analysis. Slow evaporation of a solution containing equimolar $[Zn(H_2O)_6][ClO_4]_2$ and $\mathbf{L^1}$ and an excess of $Ba(ClO_4)_2$ afforded microcrystals of $[Zn(\mathbf{L^1})(H_2O)_2\{Ba(ClO_4)_2(H_2O)_{0.75}\}][ClO_4]_2$·MeCN·0.5$Et_2O$ (**1**·MeCN·0.5Et_2O), the structure of which is shown in Figure 4. In the solid-state, $\mathbf{L^1}$ coordinates to the equatorial plane of the Zn^{II} centre via all four N-donors, whilst a further two water molecules occupy the axial positions. This arrangement generates a distorted pseudo-octahedral geometry about the Zn^{II} centre [Zn–N distances: 2.178(5)–2.237(6) Å and Zn–O distances: 2.060(5) and 2.095(5) Å] analogous to that observed by Baxter et al. for the Zn^{II} complex of the analogous crown-free ligand $\mathbf{L^2}$.[9] The ligand exhibits a shallow helical twist about the metal (N-C-C-N dihedral angle ca. 31.0°), presumably caused by unfavourable steric interaction between the methylene substituents on the central bipyridine core.[1]

The uptake of Ba^{2+} ions observed in solution is also evidenced by the crystal structure of $\mathbf{1}^{2+}$ (Table 3). The external [18]crown-6 macrocycle on $\mathbf{L^1}$ has all six O-donors directed towards the cavity interior, wherein a Ba^{2+} ion is located. The Ba–O separations lie in the range 2.803(4)–2.893(4) Å and with the two longest separations involving the methylene oxygens [Ba–$O_{(methylene)}$ 2.833(4) and 2.893(4) Å], the Ba^{2+} ion is slightly displaced away from the cavity centre and towards the outer four O-donors. The coordination sphere of the Ba^{2+} ion is supplemented by two perchlorate anions and a water molecule giving the Ba^{2+} ion a ten-coordinate geometry (on average) in the solid-state.[2]

Cadmium(II) system: The ^{1}H NMR spectra of solutions (CD_3CN, $[\mathbf{L^1}]_{tot} = 0.04$ M) containing equimolar amounts of $[Cd(H_2O)_6][ClO_4]_2$ and $\mathbf{L^1}$, before and after treatment with one equivalent of $Na(ClO_4)$, $K(ClO_4)$, $Ba(ClO_4)_2$ and $Sr(ClO_4)_2$, are shown in Figure 5. In each case the methylene -CH_2- proton signals ($4.4 \leq \delta \leq 5.4$) experience various degrees of change in both frequency and multiplicity. On addition of Na^+ ions, the -CH_2- signals merge into (relatively sharp) singlets, but neither is significantly shifted downfield from the initial average positions. The presence of K^+, Ba^{2+} or Sr^{2+} ions has a more pronounced effect; significant downfield shifts are observed ($0.2 \leq \Delta\delta \leq 0.4$) and the -$CH_2$- signals resolve into two doublets (as expected for a diastereotopic AB spin system with slow exchange on the NMR timescale).

Of particular interest is the impact which the presence of different s-block cations appears to have on the monomer/helicate equilibrium. Whereas signals in the aromatic region show only minor changes in chemical shift, the relative intensities of peaks corresponding to different species vary significantly depending on which s-block cation is added. The presence of Na^+ reduces the amount of helicate species present by about 50%, whilst the presence of K^+, Ba^{2+} or

[1] This structure has previously featured in a communication; CCDC-278718 contains the supplementary crystallographic data for this paper.[3]

[2] One of the ClO_4^- coordinates via two O-donors and was refined satisfactorily with full crystallographic site occupation, but the other is disordered over two positions with 75:25 site occupancies. In the disordered anion, the minor component acts as a bidentate O-donor ligand, whilst the major component coordinates via only one O-donor. The remaining site then becomes occupied by a (75% site occupancy) water ligand.

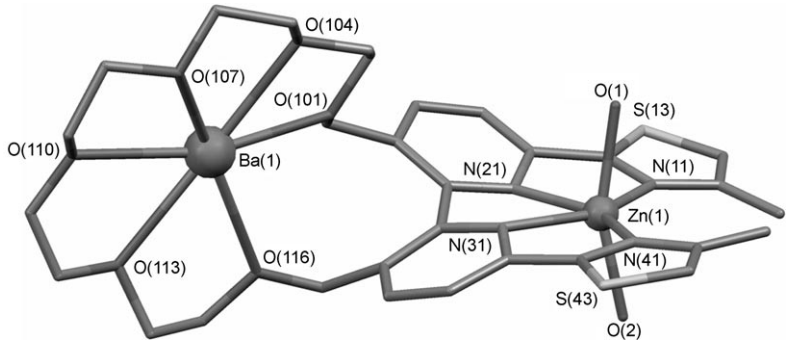

Figure 4. Solid-state structure of $[Zn(\mathbf{L^1})(H_2O)_2\{Ba(ClO_4)_2(H_2O)_{0.75}\}]^{2+}$ ($\mathbf{1}^{2+}$). Barium-bound perchlorate and water moieties have been omitted for clarity.

Table 3. Selected bond lengths [Å] and angles [°] for **1**. Ba–O distances involving oxygen atoms O(1A)–O(3) relate to the barium-bound perchlorate and water ligands.

Zn(1)–O(1)	2.095(5)	N(21)-Zn(1)-N(41)	147.23(19)	Ba(1)–O(101)	2.833(4)
Zn(1)–O(2)	2.060(5)	N(31)-Zn(1)-N(21)	71.91(18)	Ba(1)–O(104)	2.809(4)
Zn(1)–N(11)	2.237(6)	O(2)-Zn(1)-N(31)	100.2(2)	Ba(1)–O(107)	2.803(4)
Zn(1)–N(21)	2.192(5)	O(1)-Zn(1)-N(31)	97.6(2)	Ba(1)–O(110)	2.811(5)
Zn(1)–N(31)	2.178(5)	O(2)-Zn(1)-N(21)	101.8(2)	Ba(1)–O(113)	2.818(5)
Zn(1)–N(41)	2.213(5)	O(1)-Zn(1)-N(21)	91.5(2)	Ba(1)–O(116)	2.893(4)
		O(2)-Zn(1)-N(41)	86.1(2)	Ba(1)–O(1A)	2.937(6)
N(31)-Zn(1)-N(11)	147.1(2)	O(1)-Zn(1)-N(41)	90.5(2)	Ba(1)–O(1B)	2.908(5)
N(21)-Zn(1)-N(11)	75.21(19)	O(2)-Zn(1)-O(1)	160.4(2)	Ba(1)–O(2A)	2.840(6)
N(41)-Zn(1)-N(11)	137.5(2)	O(2)-Zn(1)-N(11)	86.1(2)	Ba(1)–O(2F)	2.67(3)
N(31)-Zn(1)-N(41)	75.40(19)	O(1)-Zn(1)-N(11)	83.4(2)	Ba(1)–O(3)	2.877(7)

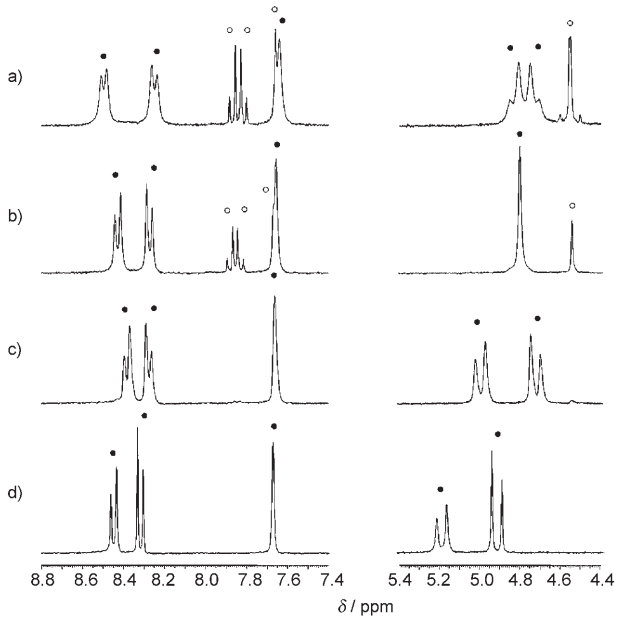

Figure 5. Selected regions of the ^{1}H NMR spectra of solutions (CD_3CN) containing equimolar amounts of a) $\mathbf{L^1}$ and $[Cd(H_2O)_6][ClO_4]_2$, b) $\mathbf{L^1}$, $[Cd(H_2O)_6][ClO_4]_2$ and $Na(ClO_4)$, c) $\mathbf{L^1}$, $[Cd(H_2O)_6][ClO_4]_2$ and $K(ClO_4)$ and d) $\mathbf{L^1}$, $[Cd(H_2O)_6][ClO_4]_2$ and $Ba(ClO_4)_2$ or $Sr(ClO_4)_2$. The symbols denote peaks assigned to single-stranded (●) and double-stranded helicate (○) species.

Sr^{2+} ions appears to eradicate virtually all traces of the dicadmium(II) helicate.

Electrospray ionisation mass spectroscopy and X-ray crystallographic studies are consistent with these observations. The mass spectrum of a solution containing equimolar $\mathbf{L^1}$, $[Cd(H_2O)_6][ClO_4]_2$ and $Ba(ClO_4)_2$ shows an intense peak at m/z 1160.4 corresponding to the single-stranded cadmium(II) cation $[Cd(\mathbf{L^1})Ba(ClO_4)_3]^+$, but no sign of any double-stranded dicadmium(II) species. In particular, the peak at m/z 1747.1 $\{[Cd_2(\mathbf{L^1})_2(ClO_4)_3]^+\}$ corresponding to the dicadmium(II) helicate (observed in the absence of Ba^{2+} ions) is no longer present.

Slow diffusion of diethyl ether vapour into a solution (MeCN) containing equimolar $[Cd(H_2O)_6][ClO_4]_2$ and $\mathbf{L^1}$ and an excess of $Ba(ClO_4)_2$ afforded microcrystals of $[Cd(\mathbf{L^1})(ClO_4)_2\{Ba(ClO_4)_2\}]$ (**2**) the structure of which is shown in Figure 6 (CCDC-637058). The complex **2** is effectively isostructural with the zinc(II) analogue ($\mathbf{1}^{2+}$), except that the two axial positions on the cadmium(II) centre are occupied by monodentate perchlorate anions leading to a charge neutral complex in the solid-state. $\mathbf{L^1}$ coordinates to the cadmium(II) centre via all four N-donors and, coupled with the axial perchlorate ligands, generates a distorted pseudo-octahedral geometry about the metal. Crystals of **2** (Table 4) were non-merohedrally twinned (see Experimental Section for details) and so a detailed analysis of the metric parameters is precluded. The data are nonetheless of sufficient quality to confirm the atomic connectivity of the complex molecule and likewise establish the presence of a Ba^{2+} ion within the external [18]crown-6 macrocycle. As with $\mathbf{1}^{2+}$ the crown ether coordinates the Ba^{2+} ion via all six O-donors, forming an equatorial belt around the metal. The remaining sites on Ba(1) are occupied by two bidentate perchlorate anions.

Mercury(II) system: As for the zinc(II) and cadmium(II) systems, the ^{1}H NMR spectra of solutions (CD_3CN, $[\mathbf{L^1}]_{tot} = 0.04$ M) containing equimolar $[Hg(H_2O)_3][ClO_4]_2$ and $\mathbf{L^1}$ were recorded before and after treatment with one equivalent of various s-block cations. Selected spectra are shown in Figure 7.

The spectrum obtained following addition of Na^+ ions (Figure 7b) shows relatively small chemical shift changes $\Delta\delta$ in the methylene and aromatic regions ($0.01 \leq \Delta\delta \leq 0.04$)

Table 4. Selected bond lengths [Å] and angles [°] for **2**.

Cd(1)–N(11)	2.274(11)	N(41)-Cd(1)-N(21)	138.1(4)	Ba(1)–O(3A)	2.842(9)
Cd(1)–N(21)	2.357(11)	N(31)-Cd(1)-N(21)	68.1(3)	Ba(1)–O(3B)	2.893(8)
Cd(1)–N(31)	2.355(9)	N(11)-Cd(1)-O(2A)	91.4(4)	Ba(1)–O(4A)	2.855(10)
Cd(1)–N(41)	2.288(14)	N(41)-Cd(1)-O(2A)	82.3(4)	Ba(1)–O(4B)	2.830(11)
Cd(1)–O(1A)	2.361(9)	N(11)-Cd(1)-O(1A)	75.1(4)	Ba(1)–O(101)	2.865(7)
Cd(1)–O(2A)	2.347(10)	N(41)-Cd(1)-O(1A)	89.0(4)	Ba(1)–O(104)	2.805(9)
		N(31)-Cd(1)-O(1A)	117.3(3)	Ba(1)–O(107)	2.809(9)
N(11)-Cd(1)-N(21)	72.5(4)	N(21)-Cd(1)-O(1A)	99.4(4)	Ba(1)–O(110)	2.809(8)
N(41)-Cd(1)-N(31)	71.5(4)	O(2A)-Cd(1)-N(21)	114.3(3)	Ba(1)–O(113)	2.785(8)
N(11)-Cd(1)-N(41)	148.4(4)	O(2A)-Cd(1)-N(31)	98.6(4)	Ba(1)–O(116)	2.813(8)
N(11)-Cd(1)-N(31)	140.1(4)	O(2A)-Cd(1)-O(1A)	138.1(4)		

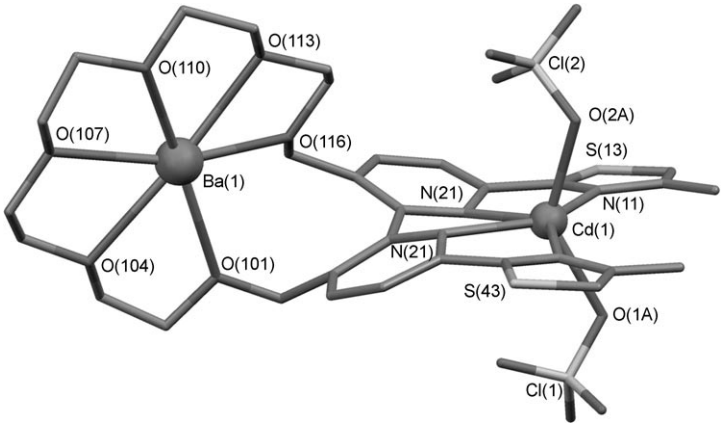

Figure 6. Solid-state structure of $[Cd(\mathbf{L^1})(ClO_4)_2\{Ba(ClO_4)_2\}]$ (**2**). Barium-bound perchlorate and water moieties have been omitted for clarity.

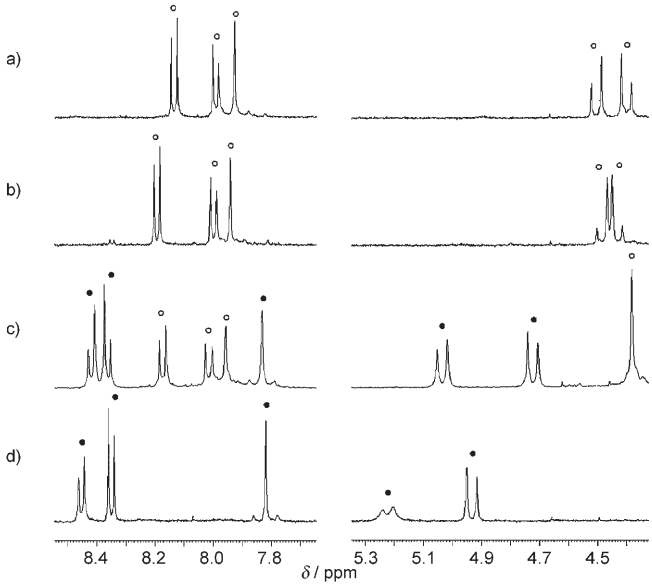

Figure 7. Selected regions of the ^{1}H NMR spectra of solutions (CD_3CN) containing equimolar amounts of a) $\mathbf{L^1}$ and $[Hg(H_2O)_3][ClO_4]_2$, b) $\mathbf{L^1}$, $[Hg(H_2O)_3][ClO_4]_2$ and $Na(ClO_4)$, c) $\mathbf{L^1}$, $[Hg(H_2O)_3][ClO_4]_2$ and $K(ClO_4)$, d) $\mathbf{L^1}$, $[Hg(H_2O)_3][ClO_4]_2$ and $Ba(ClO_4)_2$ or $Sr(ClO_4)_2$. The symbols denote peaks assigned to single-stranded (●) and double-stranded helicate (○) species.

consistent with minor coordinative perturbations caused by weak binding of Na^+ ions to [18]crown-6 macrocycles. The retention of dimercury(II) double-stranded helicate structure is supported by the appearance of peaks at *m*/*z* 2046 and 2681 in the mass spectrum, which correspond to the double-stranded dimercury(II) cations $[Hg_2(\mathbf{L^1})_2Na(ClO_4)_4]^+$ and $[Hg_2(\mathbf{L^1})_2Na_2(ClO_4)_5]^+$, respectively. Similarly, slow diffusion of diethyl ether vapour into a solution (MeCN) containing equimolar $[Hg(H_2O)_3][ClO_4]_2$, $\mathbf{L^1}$ and an excess of $Na(ClO_4)$ afforded microcrystals of $[Hg_2(\mathbf{L^1})_2\{Na(ClO_4)(MeCN)\}\{Na\}][ClO_4]_5\cdot 3\,MeCN$ (**3**·3 MeCN), the structure of which is shown in Figure 8.[3]

In the complex cation $\mathbf{3}^{5+}$ two strands of $\mathbf{L^1}$ are partitioned into bis-bidentate py-tz N-donor units by rotation of about 93° about the central py–py bond (N-C-C-N dihedral angle), allowing both to bridge the two Hg^{II} centres in the usual manner for helicates of this type.[5] The Hg–N separations are distributed over a wide range [2.107(5)–2.534(5) Å, Table 5], with the Hg^{II} centres being situated closest to the tz N-donors [$Hg–N_{(tz)}$ 2.107(5)–2.151(5) Å vs $Hg–N_{(py)}$ 2.451(5)–2.534(5) Å]. Each Hg^{II} centre in $\mathbf{3}^{5+}$ also appears to receive stabilisation from two nearby perchlorate anions; however, with relatively long $Hg–O_{(perchlorate)}$ separations in the range about 2.7–3.0 Å these separations are perhaps better described as pseudo-coordinate interactions. Both [18]crown-6 macrocycles partially coordinate sodium ions. Na(1) is seven-coordinate and bonds to five of the crown oxygens [$Na–O_{(crown\ ether)}$ separations in the range 2.351(5)–2.693(5) Å] leaving one of the methylene oxygens O(216) hypodentate. The remaining two sites are occupied by an acetonitrile molecule and a monodentate perchlorate anion. The ClO_4^- anion bridges to Na(2) in the adjacent molecule generating an infinite one-dimensional chain of μ-ClO_4^--bridged cations which propagates along the crystallographic *b* axis. Including the bridging perchlorate, Na(2) is thus five-coordinate and interacts with only the outer four oxygens of the crown ether [$Na–O_{(crown\ ether)}$ separations in the range 2.319(7)–2.545(6) Å]. The inability of the crown ethers to fully coordinate both sodium ions (via all six O-donors) is perhaps not that surprising given the size mismatch between ion and host cavity.[10]

As for the cadmium(II) system, the presence of K^+, Ba^{2+} or Sr^{2+} ions had a much more pronounced effect than sodium on the dimercury(II) helicate $[Hg_2(\mathbf{L^1})_2]^{4+}$. Treatment of a solution (CD_3CN, $[\mathbf{L^1}]_{tot} = 0.04$ M) containing equimolar $[Hg(H_2O)_3][ClO_4]_2$ and $\mathbf{L^1}$ with one equivalent of $K(ClO_4)$ resulted in the appearance of a new set of signals in

[3] This structure has previously featured in a communication (CCDC-236695 contains the supplementary crystallographic data for this paper).[2]

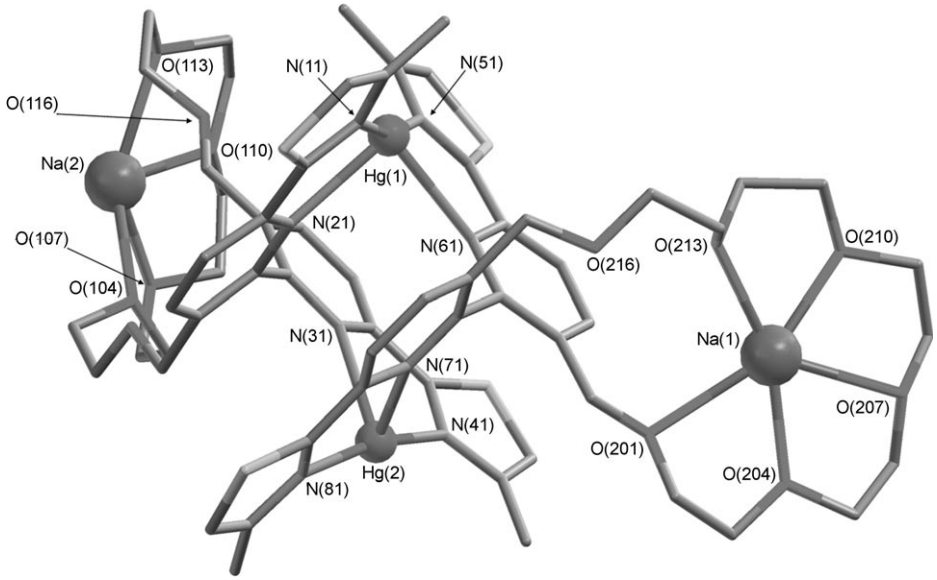

Figure 8. Complex cation $[Hg_2(\mathbf{L^1})_2\{Na(ClO_4)(MeCN)\}\{Na\}]^{5+}$ ($\mathbf{3}^{5+}$). Sodium- and mercury-bound perchlorate/acetonitrile moieties have been omitted for clarity.

Table 5. Selected bond lengths [Å] and angles [°] for **3**.

Hg(1)–N(11)	2.151(5)	N(51)-Hg(1)-N(11)	165.89(19)	Na(1)–O(201)	2.693(5)
Hg(1)–N(21)	2.451(5)	N(51)-Hg(1)-N(21)	116.03(16)	Na(1)–O(204)	2.351(5)
Hg(1)–N(51)	2.135(5)	N(51)-Hg(1)-N(61)	73.16(17)	Na(1)–O(207)	2.571(5)
Hg(1)–N(61)	2.519(5)	N(11)-Hg(1)-N(61)	118.29(17)	Na(1)–O(210)	2.391(5)
Hg(2)–N(31)	2.534(5)	N(21)-Hg(1)-N(61)	89.22(15)	Na(1)–O(213)	2.446(5)
Hg(2)–N(41)	2.107(5)	N(11)-Hg(1)-N(21)	74.07(17)	Na(2)–O(110)	2.319(6)
Hg(2)–N(71)	2.466(5)	N(41)-Hg(2)-N(71)	118.43(16)	Na(2)–O(107)	2.478(6)
Hg(2)–N(81)	2.112(5)	N(81)-Hg(2)-N(71)	73.55(17)	Na(2)–O(113)	2.534(6)
		N(41)-Hg(2)-N(31)	73.47(16)	Na(2)–O(104)	2.545(6)
		N(81)-Hg(2)-N(31)	113.98(18)		
		N(71)-Hg(2)-N(31)	88.71(14)		
		N(41)-Hg(2)-N(81)	166.86(18)		

the ^{1}H NMR spectrum, the py-tz proton chemical shifts δ of which suggest a single-stranded complex. The original set of peaks (due to the helicate) did not disappear altogether indicating the retention of substantial quantities of the double-stranded helicate (ca. 30%). On addition of $Ba(ClO_4)_2$ or $Sr(ClO_4)_2$ only one set of peaks remained, the chemical shifts of which ($7.9 \leq \delta \leq 8.5$) are entirely typical of the single-stranded (mononuclear) complex (Figure 7c).[5] However, in contrast to the K^+ case, none of the original resonances from the double-stranded helicate species remain. Likewise, the electrospray ionisation mass spectra of these solutions are dominated by peaks corresponding to molecular ions with $[Hg(\mathbf{L^1})M(MeCN)_n]^{4+}$ and $[Hg(\mathbf{L^1})M(ClO_4)_3]^+$ ($M = Ba^{2+}$ or Sr^{2+}, $n = 1$–3) formulations.

Diffusion of diethyl ether vapour into solutions (MeCN) containing equimolar $[Hg(H_2O)_3][ClO_4]_2$ and $\mathbf{L^1}$ with excess $Sr(ClO_4)_2$ or $Ba(ClO_4)_2$ afforded microcrystals of $[Hg(\mathbf{L^1})(ClO_4)\{Sr(ClO_4)_2\}]\cdot MeCN$ (**4**·MeCN) (CCDC-637059) and $[Hg(\mathbf{L^1})(ClO_4)\{Ba(ClO_4)_2\}]$ (**5**), respectively. Significantly different unit cell parameters indicate that the crystals are not isomorphous; yet to all intents and purposes the complex molecules are isostructural and show the expected single-stranded structures (Figure 9).[4]

Like their zinc(II) and cadmium(II) counterparts ($\mathbf{1}^{2+}$ and **2**), the solid-state structures show a near planar ligand coordinating to the Hg^{II} centres via the py-tz N-donors, whilst all six oxygens in the crown ether coordinate the s-block dication. Metal–$O_{(crown\ ether)}$ separations to the Sr^{2+} ion (in **4**) are generally shorter than those to the Ba^{2+} ion (Table 6), reflecting the contraction in ionic radius on ascending the Group II dications. In **4** the two Sr–$O_{(methylene)}$ separations are significantly longer than the remaining etherate interactions, displacing the Sr^{2+} ion away from the cavity centre and towards the outer O-donors.

Copper(I) system: The addition of $Na(ClO_4)$ or $Ba(ClO_4)_2$ to a solution (CD_3CN, $[\mathbf{L^1}]_{tot} = 0.04$ M) containing the dicopper(I) helicate $[Cu_2(\mathbf{L^1})_2]^{2+}$ caused significant downfield shifts ($0.2 \leq \Delta\delta \leq 0.5$) for the methylene protons, indicative of s-block cation binding by the

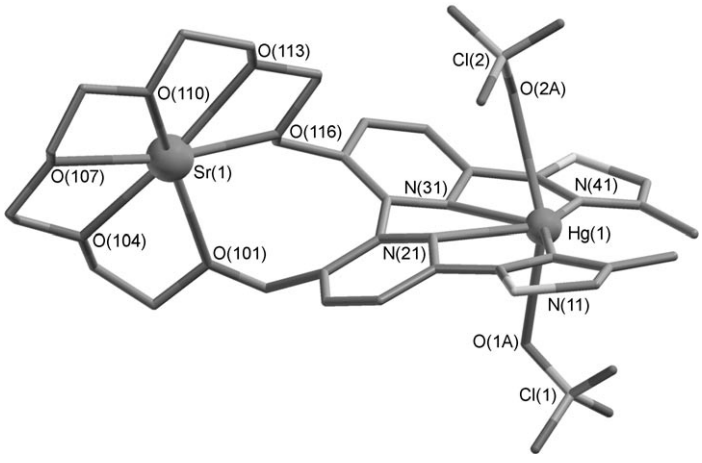

Figure 9. Solid-state structure of $[Hg(\mathbf{L^1})(ClO_4)_2\{Sr(ClO_4)_2\}]$ (**4**). Strontium-bound perchlorate moieties have been omitted for clarity.

[4] This structure has previously featured in a communication (CCDC-236694 contains the supplementary crystallographic data for this paper).[2]

Table 6. Selected bond lengths [Å] and angles [°] for **4** and **5**.

	M = Sr	M = Ba		M = Sr	M = Ba
Hg(1)–N(11)	2.158(9)	2.254(12)	N(11)-Hg(1)-N(41)	155.1(4)	152.5(5)
Hg(1)–N(21)	2.488(8)	2.473(13)	N(11)-Hg(1)-N(21)	71.4(3)	72.2(4)
Hg(1)–N(31)	2.535(10)	2.461(12)	N(41)-Hg(1)-N(21)	133.4(3)	135.3(5)
Hg(1)–N(41)	2.164(9)	2.247(11)	N(11)-Hg(1)-N(31)	134.4(3)	135.3(4)
Hg(1)–O(1A)	2.737(9)	2.568(15)	N(41)-Hg(1)-N(31)	70.4(3)	71.5(5)
Hg(1)–O(2A)	2.862(9)	2.650(13)	N(21)-Hg(1)-N(31)	63.0(3)	64.5(4)
M–O(101)	2.876(7)	2.898(10)	N(41)-Hg(1)-O(1A)	81.54(4)	74.7(4)
M–O(104)	2.616(7)	2.800(10)	N(11)-Hg(1)-O(1A)	99.94(4)	95.4(5)
M–O(107)	2.697(7)	2.855(11)	N(31)-Hg(1)-O(1A)	77.31(4)	92.6(4)
M–O(110)	2.672(7)	2.763(12)	N(21)-Hg(1)-O(1A)	88.11(4)	113.9(4)
M–O(113)	2.692(7)	2.791(9)	N(41)-Hg(1)-O(2A)	80.00(4)	98.4(5)
M–O(116)	2.765(7)	2.812(10)	N(11)-Hg(1)-O(2A)	108.87(4)	77.5(5)
M–O(3A)	2.677(9)	2.904(11)	N(31)-Hg(1)-O(2A)	69.42(4)	112.8(4)
M–O(3B)	2.727(10)	2.845(12)	N(21)-Hg(1)-O(2A)	84.02(4)	91.4(5)
M–O(4A)	2.679(8)	2.861(12)	O(1D)-Hg(1)-O(2A)	145.76(4)	150.5(4)
M–O(4B)	2.724(8)	2.852(12)			

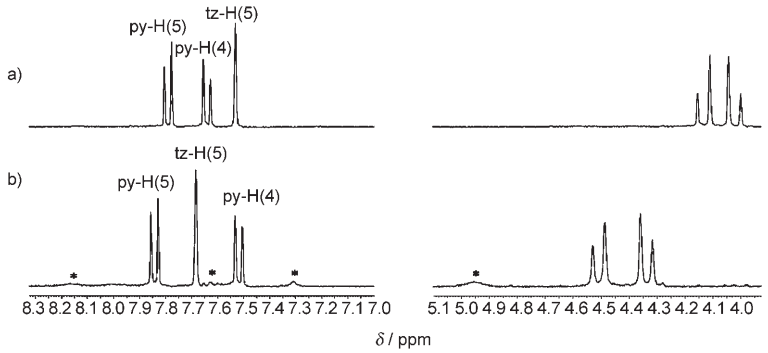

Figure 10. Selected regions of the ^{1}H NMR spectra of solutions (CD_3CN) containing equimolar amounts of a) $\mathbf{L^1}$ and $[Cu(MeCN)_4][PF_6]$ and b) $\mathbf{L^1}$, $[Cu(MeCN)_4][PF_6]$ and $Ba(ClO_4)_2$. Peaks due to the (possible) single-stranded species are marked with an asterisk.

crown ether. The aromatic py-tz protons also experienced chemical shift changes $\Delta\delta$, but the overall range for these protons ($7.5 \leq \delta \leq 7.9$) remained largely unaffected by either Na^+ or Ba^{2+} ions. The presence of Ba^{2+} ions did, however, cause significant alterations in the relative positions of the py-tz proton signals (Figure 10b); the tz-H(5) signal moved downfield and the py-H(4) moved upfield by approximately δ 0.2 ppm. The appearance of another set of very weak signals was also observed, but the low concentration at which the corresponding species is present makes it difficult to speculate on whether it is a similar single-stranded complex to those formed on addition of Ba^{2+} ions to the Group XII helicates. The retention of a dicopper(I) helicate structure was supported by the observation of NOE signals between the methylene and methyl protons in the NOESY spectrum.

Diffusion of diethyl ether vapour into solutions (MeCN) containing equimolar $[Cu(MeCN)_4][PF_6]$, $\mathbf{L^1}$ and excess $Na(ClO_4)$ or $Ba(ClO_4)_2$ afforded microcrystals of $[Cu_2(\mathbf{L^1})_2\{Na(ClO_4)_2\}\{Na(MeCN)\}][ClO_4]_2 \cdot 0.5\,MeCN \cdot 0.5\,NaClO_4$ ($\mathbf{6} \cdot 0.5\,MeCN \cdot 0.5\,NaClO_4$) (CCDC-637060) and $[Cu_2(\mathbf{L^1})_2\{Ba(ClO_4)_2\}_2]$-$[ClO_4]_2 \cdot 2\,MeCN \cdot 0.5\,Et_2O$ ($\mathbf{7} \cdot 2\,MeCN \cdot 0.5\,Et_2O$).[5] The solid-state structure of **6** is shown in Figure 11 and selected metric parameters for both complexes are listed in Table 7.

The complex cations $\mathbf{6}^{2+}$ and $\mathbf{7}^{2+}$ have dicopper(II) double-stranded helicate structures in which the Cu^I centres are coordinated by one bis-bidentate py-tz N-donor unit from each ligand to give distorted tetrahedral geometries. The Cu–N separations fall in the range 1.985(7)–2.158(8) Å (Table 7) and a similar pattern of short Cu–$N_{(tz)}$ and long Cu–$N_{(py)}$ separations is observed in both complexes.

The remote [18]crown-6 macrocycles all accommodate s-block metal cations. In $\mathbf{6}^{2+}$ one crown ether binds Na(1) via all six oxygens [Na–O distances 2.395(5)–2.653(4) Å] whilst the other binds Na(2) via only five [Na–O distances 2.401(5)–2.458(4) Å]. The Na^+ ions, however, are both seven-coordinate due to the additional coordination of an acetonitrile ligand to Na(1) and two perchlorate anions to Na(2). In order to coordinate Na(1) via all six O-donors, the [18]crown-6 fragment adopts a curved saddle-like conformation, making the host cavity three-dimensional in appearance. In contrast, the crown ether which binds to Na(2) resembles more closely those in the dimercury(II) helicate $\mathbf{3}^{5+}$, wherein the coordinating O-donors are reasonably co-planar and form an equatorial belt around the cation. With the hypodentate oxygen atom lying out of this plane, the ring can effectively transform into a smaller [15]crown-5 macrocycle better suited for sodium binding. Moreover, by preferential coordination of only the outer oxygens, both Na^+ ions are also located further away from the dicopper(I) core of the complex.

In $\mathbf{7}^{2+}$ the [18]crown-6 macrocycles coordinate Ba^{2+} ions via all six O-donors with Ba–O separations in the range 2.760(8)–2.978(12) Å. Each of the Ba^{2+} ions are additionally stabilised by two perchlorate anions [Ba-$O_{(perchlorate)}$ distances 2.800(11)–2.960(10) Å] giving both ten-coordinate geometries in the solid-state.

The structural feature which most distinguishes the dicopper(I) cores of helicates $\mathbf{6}^{2+}$ and $\mathbf{7}^{2+}$ is an increase in helical pitch of about 0.45 Å which accompanies replacement of the

[5] This structure has previously featured in a communication (CCDC-278717 contains the supplementary crystallographic data for this paper).[3]

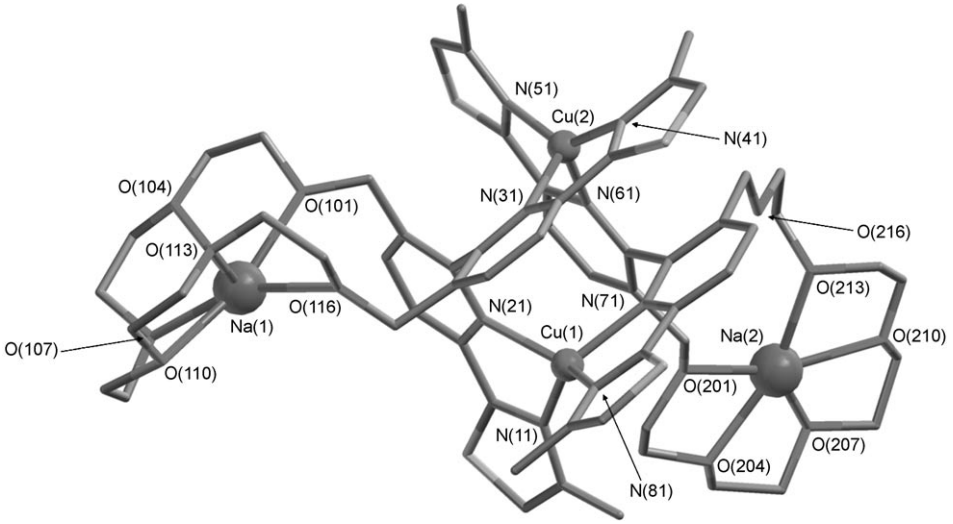

Figure 11. Solid-state structure of the complex cation $\mathbf{6}^{2+}$. Sodium-bound acetonitrile and perchlorate moieties have been omitted for clarity.

Table 7. Selected bond lengths [Å] and angles [°] for **6** and **7**.

	M = Na	M = Ba		M = Na	M = Ba
Cu(1)–N(11)	2.009(4)	2.026(7)	N(81)-Cu(1)-N(11)	130.4(3)	128.91(17)
Cu(1)–N(21)	2.090(4)	2.109(7)	N(81)-Cu(1)-N(21)	135.2(2)	128.04(16)
Cu(1)–N(71)	2.074(4)	2.158(8)	N(11)-Cu(1)-N(21)	81.8(3)	81.42(16)
Cu(1)–N(81)	2.000(4)	2.002(9)	N(81)-Cu(1)-N(71)	80.9(2)	81.25(16)
Cu(2)–N(31)	2.126(4)	2.155(7)	N(11)-Cu(1)-N(71)	126.7(2)	128.71(16)
Cu(2)–N(41)	1.998(4)	1.985(7)	N(21)-Cu(1)-N(71)	105.3(2)	113.92(15)
Cu(2)–N(51)	2.003(4)	2.032(9)	N(41)-Cu(2)-N(51)	130.1(3)	138.28(18)
Cu(2)–N(61)	2.106(4)	2.102(7)	N(41)-Cu(2)-N(61)	135.84(19)	127.86(16)
M(1)–O(101)	2.501(4)	2.926(12)	N(51)-Cu(2)-N(61)	81.8(3)	81.10(16)
M(1)–O(104)	2.521(5)	2.765(9)	N(41)-Cu(2)-N(31)	80.7(3)	80.92(17)
M(1)–O(107)	2.536(5)	2.829(9)	N(51)-Cu(2)-N(31)	126.9(2)	122.51(16)
M(1)–O(110)	2.576(5)	2.795(12)	N(61)-Cu(2)-N(31)	104.9(3)	107.42(15)
M(1)–O(113)	2.395(5)	2.786(9)			
M(1)–O(116)	2.653(4)	2.881(10)			
M(2)–O(201)	2.418(4)	2.978(12)			
M(2)–O(204)	2.401(5)	2.760(8)			
M(2)–O(207)	2.458(4)	2.807(8)			
M(2)–O(210)	2.428(5)	2.852(12)			
M(2)–O(213)	2.438(4)	2.840(8)			
M(2)–O(216)	–	2.791(9)			

crown ether-bound sodium monocations with barium dications. The Cu···Cu separations in $\mathbf{6}^{2+}$ and $\mathbf{7}^{2+}$ are 4.529(1) and 4.984(2) Å, respectively, and, although these parameters may be susceptible to variations in crystal packing environment, a difference of this magnitude ($\Delta \approx 0.45$ Å) invokes strong contributions from the presence of Na^+/Ba^{2+} ions in the crown ether macrocycles in the respective complexes.

The variation in helical pitch seen in the solid-state also has a bearing on the py-tz protons on $\mathbf{L^1}$; as the internuclear separation increases the positions of the py-tz protons on one strand relative to the shielding regions on the other strand undergo considerable change (Figure 12). The tz-H(5) proton is moved further away from the shielding region of the py ring, whilst py-H(4) and H(5) move into and out of (respectively) that of the overlapping tz ring. If retained in solution, it is entirely plausible that these distortions are responsible for the changes in chemical shift order observed for the py-tz ^{1}H NMR signals after addition of $Ba(ClO_4)_2$.

Discussion

The solution-phase complexes of $\mathbf{L^1}$ with the Group XI and XII mono- and dications respond to the presence of s-block cations in a variety of different ways. In all cases, ^{1}H NMR spectra, mass spectra and X-ray crystallography provide qualitative evidence for the binding of the s-block cations by the external [18]crown-6 macrocycles on $\mathbf{L^1}$, but of greater interest perhaps are the structural and topological changes which appear to accompany these binding events. The dinuclear double-stranded helicates formed with Cd^{II} and Hg^{II} dications, for example, disassemble into single-stranded complexes in which transition and s-block cations reside in the N- and O-donor binding domains, respectively. The changes observed for the dicopper(I) helicate are more subtle; rather than causing a change in gross molecular structure, the binding of s-block cations appears to influence the internuclear separation or helical pitch of the helicate. Indeed, it is only the mononuclear complexes $[M(\mathbf{L^1})]^{2+}$ ($M = Zn^{II}$, Cd^{II}) which are (structurally) little affected by crown ether complexation.

Within the boundaries of the experimental data obtained, definitive explanations for these phenomena are unattainable. It is likely that each system is under the combined influence of numerous different forces; however, the ^{1}H NMR measurements and solid-state structures do present the opportunity to monitor the effects of some of the less elusive variables such as s-block and transition metal cation size and charge, overall complex charge, ligand conformation and sterics.

The extent to which s-block cation binding influences a given system, be it by helicate disassembly or pitch modulation, is closely related to the size and charge of the s-block cation used. The effect of size is illustrated by the respective impacts of adding Na^+ and K^+ ions to either the cadmium(II) or mercury(II) systems. In both cases, the larger K^+

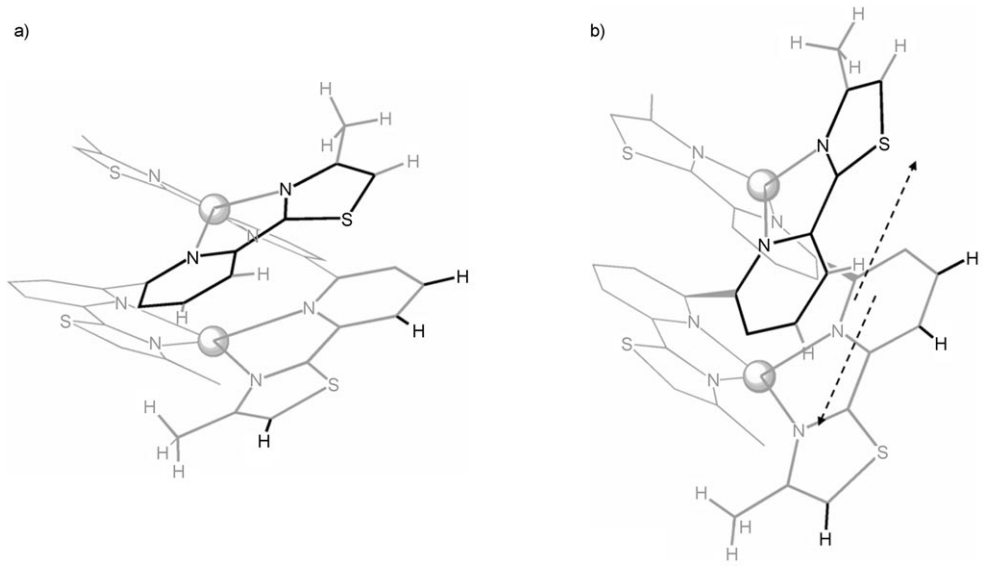

Figure 12. Schematic diagram illustrating how increasing the internuclear separation alters the positions of the py-tz protons on one strand relative to the shielding regions on the other strand. The helicate in a) has a Cu···Cu separation of ca. 3.5 Å, whereas in b) the Cu···Cu separation is increased to ca. 4.5 Å.

ion ($r \approx 1.33$ Å) commands a much more pronounced response than the Na^+ ion ($r \approx 0.95$ Å) in shifting the equilibrium towards the single-stranded species. When the impacts of ions of similar size but different oxidation state are compared, the effect of charge becomes apparent. Between K^+ and Ba^{2+}, a significantly more pronounced response is observed for the dicationic Ba^{2+} ion. That Sr^{2+} ($r \approx 1.15$ Å) also exerts a greater influence than K^+ tends to suggest charge as the more dominating factor. Similar trends begin to emerge for helical pitch modulation effects encountered for the Group XI helicates, though structural evidence is limited to the solid-state complexes of dicopper(I) helicates $\mathbf{6}^{2+}$ and $\mathbf{7}^{2+}$.

The above observations correlate with trends in stability constant reported by Yam et al. for the s-block cation complexes of a related ditopic ligand which contains an [18]crown-6 macrocycle appended to a pyridyl-imine N-donor ligand.[11] In acetonitrile, the stability constants were found to increase in the order $Li^+ < Na^+ < K^+ < Ba^{2+}$, with the highest value of $\log K_s \approx 4.69$ for Ba^{2+} being rationalised on the grounds of its high charge density.[11] It is worth noting, however, that a direct comparison is not wholly appropriate because the impact (helicate disassembly or pitch modulation) that a given s-block cations exerts on the present $\mathbf{L^1}$ systems is likely a reflection of two closely related factors; namely, the affinity of that cation for the crown ether host and the mechanism by which it induces change in the transition metal (helicate) complex. One such mechanism could involve the crown ether binding site exerting allosteric control over the py-tz N-donor domains.[12] Effectively, conformational changes in the crown ether, caused by complexation of the s-block cation, are mechanically coupled to the py-tz N-donor domains in such a way as to impede the necessary partitioning (into bis-bidentate py-tz units) for helicate assembly to occur, that is, the py–py bonds are forced to be near coplanar. Viewed from a different (but equally valid) perspective, the crown ether conformation in the single-stranded complex may simply be more appropriate for accommodating an s-block cation; the resulting free energy difference between crown ether complexation in the helicate versus single-stranded ligand conformations providing a thermodynamic driving force for disassembly.

The limitation of this mechanism is that it cannot be reconciled with the respective effects that s-block cation binding has on both the Group XI and XII helicates. In one case helicate disassembly occurs, leading to a decrease of up to 60° in the central py–py dihedral angle so that the py-tz domains can coordinate in a near planar tetradentate fashion (Figure 13a). In the case of the dicopper(I) helicate, the observed helical pitch modulation requires if anything an increase in py–py dihedral angle. Indeed, comparison of the solid-state structures of $\mathbf{6}^{2+}$ and $\mathbf{7}^{2+}$ shows an increase of about 20° in py–py dihedral angle on replacing the crown ether bound Na^+ for Ba^{2+} cations. We have previously observed similar trends in a series of dicopper(II) double-stranded helicates, whose solid-state internuclear separations were found to depend on the size and charge of an s-block cation located in a remote crown ether binding site.[4]

This disparity invokes the influences of other factors, arguably the most apparent of which is the accumulation of charge in the s-block cation bound complexes, that is, both helicate disassembly and pitch increase could be the result of electrostatic repulsion effects. Placing two crown ether-bound Ba^{2+} ions in close proximity to the dicopper(I) helicate core increases electrostatic repulsion within the complex and encourages the N-donor bound Cu^I ions to move further apart. This response will manifest in several areas of

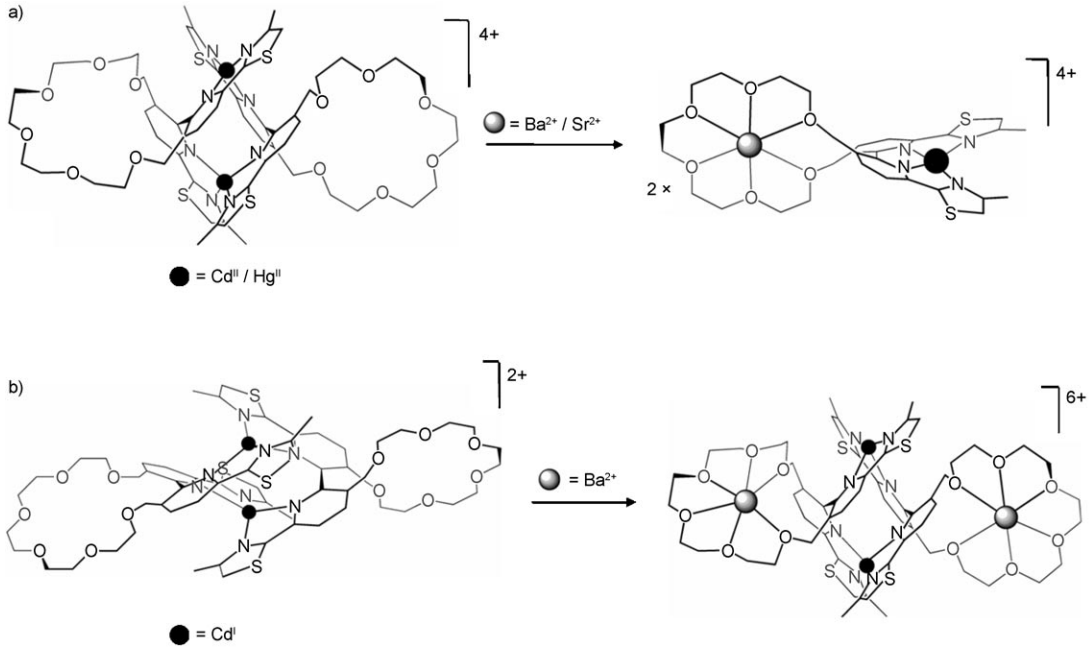

Figure 13. Schematic diagram illustrating the effect that s-block cation binding has on a) the Group XII dinuclear helicates and b) the Group XI dinuclear helicates.

the complex; obviously the internuclear (transition metal) separation will increase, but so too will the py–py dihedral angles since the coordinating py-tz arms will have to compensate for the new Cu···Cu separation. For the Group XII helicates, however, the effect of introducing s-block cations (in particular Ba^{2+}/Sr^{2+}) is much more severe because of the already high charge associated with the dicadmium(II) or dimercury(II) helicate cores (4+ vs 2+ in the double-stranded Group XII and Group XI helicates, respectively). Instead of forming the highly charged 8+ cation $[M_2(\mathbf{L^1})_2\{M'\}_2]^{8+}$ ($M = Cd^{II}$ or Hg^{II} and $M' = Ba^{2+}$ or Sr^{2+}), the binding of Ba^{2+} or Sr^{2+} ions by the crown ethers causes a Coulombic fission to occur and the helicate disassembles into two single-stranded heterodinuclear species $[M(\mathbf{L^1})\{M'\}]^{4+}$ ($M = Cd^{II}$ or Hg^{II} and $M' = Ba^{2+}$ or Sr^{2+}) each of which carries an overall 4+ charge. The addition of singly charged Na^+ ions does not instigate as pronounced a change because, not only will the resulting complex $[M_2(\mathbf{L^1})_2\{Na\}_2]^{6+}$ ($M = Cd^{II}$ or Hg^{II}) have a lower (6+) charge, the smaller monocationic Na^+ ion may not require stabilisation from all six O-donors in the crown ether. Indeed, as seen in the crystal structures of $\mathbf{6}^{2+}$ and $\mathbf{3}^{5+}$, the Na^+ ions are more often that not bound by only the outer four or five oxygens in the crown ether, placing them further away from the transition metal core than, for example, the ten-coordinate Ba^{2+} ions in $\mathbf{7}^{2+}$. That the addition of K^+ ions has a more pronounced effect on the dicadmium(II)/dimercury(II) systems may simply reflect its smaller host/guest size-mismatch (cf. Na^+) and correspondingly higher affinity for the [18]crown-6 macrocycle in $\mathbf{L^1}$.

In conclusion, whether by conferring additional charge or imposing conformational restrictions, the binding of Ba^{2+} or Sr^{2+} ions to the [18]crown-6 macrocycle in $\mathbf{L^1}$ renders the ligand inappropriate for sustaining a helicate structure with the Group XII dications. The effect that s-block cation binding has on the dicopper(I) helicate is more subtle; instead of inducing disassembly, the binding of Ba^{2+} ions causes changes in the supramolecular micro-architecture such as internuclear separation and ligand partitioning (py–py dihedral angle). These phenomena are summarised in Figure 13.

Experimental Section

Characterisation and physical measurements: Electrospray ionisation mass spectra were recorded on either a continual-flow VG Quattro II triple quadrupole mass spectrometer (with Z-spray source and cone-voltages in the range 25–40 V) or a Bruker-Daltronics Apex 4e 7.0T (FT-MS) instrument. Analytes were dissolved in acetonitrile or nitromethane at concentrations of about 0.1 mg mL^{-1}. One dimensional ^{1}H NMR spectra were recorded on Jeol GX400 or Jeol GX270 spectrometers. Two dimensional (NOESY) spectra were recorded on a Jeol GX400 spectrometer.

X-ray crystallography: The crystal structures of **1**,[3] **3**,[2] **5**[2] and **7**[3] have previously been reported in preliminary communications. For all other structural analyses reported herein, crystals were visually inspected for defects and singularity under a binocular microscope fitted with a polarising attachment. Suitable crystals were then coated with epoxy resin, mounted on a glass fibre and quickly transferred to a Bruker-AXS PROTEUM or APEX (CCD area detector) diffractometer under a stream of cold N_2 gas. Preliminary scans were employed to assess crystal quality, lattice symmetry, ideal exposure time prior to collecting a sphere or hemisphere (for low- and high-symmetry crystal systems, respectively) of diffraction intensity data using SMART operating software.[13] Intensities were then integrated from several series of exposures (each exposure covering 0.3° in ω), merged and corrected for Lorentz and polarisation effects using SAINT software.[14] Solutions were generated by conventional heavy atom Patterson or direct methods and refined by full-matrix

non-linear least squares on all F^2 data, using SHELXS-97 and SHELXL software, respectively (as implemented in the SHELXTL suite of programs).[15] Empirical absorption corrections were applied based on multiple and symmetry-equivalent measurements using SADABS[16] and, where stated, the scattering contributions from diffuse solvent moieties were removed using the SQUEEZE function in PLATON.[17] All structures were refined until convergence (max shift/esd < 0.01) and in each case, the final Fourier difference map showed no chemically sensible features. Crystallographic refinement parameters for **2**, **4** and **6** are summarised in Table 8.

Refinement details for $[Cd(L^1)(ClO_4)_2\{Ba(ClO_4)_2\}]$ (2): The crystal structure of **2** was solved in the centrosymmetric space group $P\bar{1}$, though an unsatisfactory final $R1$ value (of ca. 15%), refinement instability and the presence of large residual features in the electron density map (ca. 1 Å away from the heavy metals) indicated substantial systematic error in the data. Indeed, analysis of the diffraction intensity data using GEMINI[18] suggested that crystals of **2** were non-merohedrally twinned, with the two major twin domains being related by a two-fold rotation about the crystallographic c axis. The intensity data were thus re-integrated against the orientation matrices for both twin domains and combined in HKLF 5 format allowing the original solutions to be refined against all non-merged data. This resulted in a decrease of ca. 5% in the final $R1$ values and significant reductions in both the size of the residual electron density peaks surrounding heavy metal ions and the esds associated with the various metric parameters (bond lengths and angle etc.). A number of atoms was still unstable when refined with anisotropic displacement parameters and so soft (anisotropic) displacement parameter restraints were applied. The quality of the crystal structure was nonetheless still very poor and we note that it merits no further use than establishing the connectivity of the complex cation.

Refinement details for $[Cu_2(L^1)_2\{Na(ClO_4)_2\}\{Na(MeCN)\}][ClO_4]_2\cdot 0.5\,MeCN\cdot 0.5\,NaClO_4$ ($6\cdot 0.5\,MeCN\cdot 0.5\,NaClO_4$): The complex molecule contained regions of disorder in a peripherally bound perchlorate anion and one of the crown ether macrocycles. In both regions the disorder was resolved into two components (60:40 site occupancy in each case), the atoms of which were modeled using positional and (anisotropic) displacement parameter restraints (SIMU, ISOR, SADI and DFIX). Elsewhere in the asymmetric unit, two interstitial perchlorates were resolved into two closely related positions. One of these, $ClO_4(3)$, was refined satisfactorily with only soft anisotropic displacement parameter restraints (ISOR and SIMU), whilst the two components of the more diffuse anion required extensive geometric restraints (DFIX). All atoms in the latter perchlorate were refined with isotropic displacement parameters and, for two overlapping oxygen positions, these were fixed at a value of 0.06 Å^2. Further inspection of the Fourier difference map revealed several other features; a highly disordered acetonitrile molecule, several discreet peaks in the range 2–4 e Å^{-3} and what appeared to be an additional perchlorate anion. In the latter, the positions of the oxygen atoms were poorly defined as a likely result of disorder, but the central Cl atom was satisfactorily refined with ca. 50% site occupancy. We believe this anion to be associated with the presence of a $NaClO_4$ co-crystallate rather than evidence for partial substitution of either Cu^I centres by Cu^{II} in the complex cation because, i) analysis of the mean-square-displacement amplitudes shows [d^2] values in the range 8–70 $\times 10^{-4}$ Å^2, consistent with a high level of positional order in the Cu–N coordination bonds[19] and ii) several discreet electron density peaks (2–4 e Å^{-3}) were found nearby and could well correspond to a disordered Na^+. In our final model, we have removed the scattering contributions from all of these diffuse moieties using the SQUEEZE routine in PLATON. The empirical formula is thus an estimate and expresses an additional about 0.5 × acetonitrile molecule and 0.5 × $NaClO_4$ per complex cation.

Table 8. Crystallographic refinement parameters for **2**, **4** and **6**.

	2	**4**·MeCN	**6**·0.5 MeCN·0.5 $NaClO_4$
empirical formula	$C_{30}H_{36}BaCdCl_4N_4O_{22}S_2$	$C_{32}H_{39}Cl_4HgN_5O_{22}S_2Sr$	$C_{63}H_{76.5}Cl_{4.5}Cu_2N_{9.5}Na_{2.5}O_{30}S_4$
F_w	1260.29	1339.81	1919.16
T [K]	100(2)	100(2)	100(2)
λ [Å]	1.54178	0.71073	0.71073
crystal system	triclinic	triclinic	triclinic
space group	$P\bar{1}$	$P\bar{1}$	$P\bar{1}$
unit cell dimensions			
a [Å]	8.8197(4)	8.6527(17)	14.191(3)
b [Å]	9.5862(4)	15.845(3)	14.406(3)
c [Å]	26.2374(11)	16.633(3)	20.260(4)
α [°]	89.593(3)	91.91(3)	82.25(3)
β [°]	89.251(3)	99.72(3)	84.67(3)
γ [°]	76.039(3)	97.63(3)	89.49(3)
V [Å^3]	2152.57(16)	2224.2(8)	4086.1(14)
$Z(Z')$	2(1)	2(1)	2(1)
ρ_{calcd} [Mg m^{-3}]	1.944	2.001	1.560
μ [mm^{-1}]	15.005	5.070	0.869
$F(000)$	1248	1320	1974
crystal size [mm]	0.2 × 0.05 × 0.05	0.2 × 0.05 × 0.05	0.3 × 0.2 × 0.05
θ range for data collection [°]	1.68 to 70.05	1.75 to 27.481.43 to 27.48	
index ranges	$-10 \le h \le 10$ $-11 \le k \le 11$ $-31 \le l \le 31$	$-11 \le h \le 11$ $-20 \le k \le 20$ $-21 \le l \le 21$	$-18 \le h \le 18$ $-18 \le k \le 18$ $-26 \le l \le 26$
reflns collected	15914	24617	47079
independent reflections	15914	10011 [$R_{int} = 0.1299$]	18689 [$R_{int} = 0.0502$]
data/restraints/parameters	15914/73/584	10011/0/607	18689/191/1079
GoF on F^2			
S	1.264	0.901	0.910
R indices [for 3821 reflections with $I > 2\sigma(I)$][a,b]			
$R1$	0.1103	0.0791	0.0740
$wR2$	0.2800	0.1825	0.2021
R indices (for all 4570 data)[a,b]			
$R1$	0.1151	0.1082	0.1127
$wR2$	0.2875	0.1927	0.2281
weighting scheme[b]			
a	0.2000	0.0859	0.1556
b	0.0000	0.0000	0.0000
largest diff. peak and hole [e Å^{-3}]	3.293 and −2.856	4.206 and −4.290	1.852 and −1.000

[a] Structure was refined on F_o^2 using all data; the value of R_1 is given for comparison with older refinements based on F_o with a typical threshold of $F \ge 4\sigma(F)$. [b] $wR_2 = [\Sigma[w(F_o^2 - F_c^2)^2]/\Sigma w(F_o^2)^2]^{1/2}$ where $w^{-1} = [\sigma^2(F_o^2) + (aP)^2 + bP]$ and $P = [\max(F_o^2, 0) + 2F_c^2]/3$.

Ligand synthesis: Ligand $\mathbf{L^1}$ was prepared according to procedure outlined in Scheme 1.

3,3′-([18]Crown-6)-2,2′-bipyridine: The starting material 2,2′-bipyridine-3,3′-dimethanol was prepared using the literature method.[20] 2,2′-Bipyridine-3,3′-

dimethanol (0.80 g, 3.77 mmol) and NaH (0.72 g, 8 equiv, 30.16 mmol) were stirred at 50 °C for 1 h in dry DMF (35 mL) under nitrogen. To this was then added slowly a solution of penta(ethylene glycol) di-*p*-toluenesulfonate (2.3 g, 1.1 equiv, 4.10 mmol) in dry DMF (10 mL) via syringe and the heating maintained for 12 h. On completion, methanol (15 mL) was added to react with any excess NaH and the solvent was removed under reduced pressure leaving a green residue. This was taken up in water (50 mL) and extracted into CH_2Cl_2 (3×200 mL). The solvent was then evaporated to give 3,3′-([18]crown-6)-2,2′-bipyridine as a crude green oil. This oil was then purified by column chromatography (10% MeOH in CH_2Cl_2, silica gel) to give a light amber coloured oil which solidified on standing (0.63 g, 1.51 mmol, 41%). ^{1}H NMR (400 MHz, $CDCl_3$): δ = 8.55 (dd, 2H, J=4.9, 1.7 Hz, py H^6), 7.96 (dd, 2H, J=7.8, 1.7 Hz, py H^4), 7.35 (dd, 2H, J=7.8, 4.9 Hz, py H^5), 4.56, 4.50 (AB q, 4H, J=12.7 Hz, -CH_2-), ≈3.5 ppm (m, 20H, cr); ^{13}C{^{1}H} NMR (400 MHz, $CDCl_3$): δ = 155.9 (py), 147.3 (py), 136.6 (py), 133.2 (py), 122.94 (py), 70.5 (cr), 70.4 (cr), 70.3 (cr), 70.1 (cr), 70.0 (cr), 69.4 ppm (cr); ESI-MS: m/z: 419.1 $[M+H]^+$; elemental analysis calcd (%) for $C_{22}H_{30}N_2O_6$: C 64.1, H 7.2, N 6.7; found: C 64.9, H 6.1, N 6.5.

3,3′-([18]Crown-6)-2,2′-bipyridine-*N*,*N*′-dioxide: 3,3′-([18]crown-6)-2,2′-bipyridine (0.60 g, 1.44 mmol) was dissolved in CH_2Cl_2 (20 mL) and reacted with *m*CPBA (0.621 g, 3.60 mmol). The reaction was followed by TLC (Al_2O_3) and on completion, the solvent was removed under vacuum (**CAUTION**: N-oxides are potentially explosive) leaving the crude *N*,*N*′-dioxide as a white solid. This was then purified by column chromatography (10% MeOH in CH_2Cl_2, Al_2O_3) to give the title compound as a white solid (0.63 g, 97%). ^{1}H NMR (400 MHz, $CDCl_3$): δ = 8.25 (dd, 2H, J=6.3, 1.0 Hz, py H^6), 7.52 (d, 2H, J=7.8 Hz, py H^4), 7.38 (dd, 2H, J=7.8, 6.8 Hz, py H^5), 4.40, 4.31 (AB q, 4H, J=12.7 Hz, -CH_2-), ≈3.5 ppm (m, 20H, cr); ^{13}C{^{1}H} NMR (100 MHz, $CDCl_3$): δ = 140.3 (py), 139.5 (py), 138.4 (py), 126.1 (py), 125.3 (py), 70.8 (cr), 70.7 (cr), 70.6 (4C, cr), 70.3 (cr), 69.0 ppm (cr); HR CI-MS: m/z: calcd for $C_{22}N_2H_{31}O_8$: 451.208041; found: 451.207542 $[M+H]^+$ (deviation: 1.1 ppm); elemental analysis calcd (%) for $C_{22}H_{30}N_2O_8$: C 58.7, H 6.7, N 6.2; found: C 59.6, H 6.7, N 5.9.

6,6′-Dicyano-3,3′-([18]crown-6)-2,2′-bipyridine: Benzoyl chloride (0.56 g, 4.0 mmol) and TMSCN (0.35 g, 4.0 mmol) were added to a solution of 3,3′-([18]crown-6)-2,2′-bipyridine-*N*,*N*′-dioxide (0.60 g, 1.33 mmol) in CH_2Cl_2 (50 mL). After heating at reflux for 4 h, a further portion of benzoyl chloride (0.56 g, 4.0 mmol) and TMSCN (0.35 g, 4.0 mmol) were added. Heating was maintained for a further 4 h. The solution was then allowed to cool, washed with $NaHCO_{3(aq)}$ (2×50 mL), dried and the solvent removed under reduced pressure. The residual brown oil was purified by column chromatography (1% MeOH in CH_2Cl_2, Al_2O_3) to give the title compound as a colourless oil (0.37 g, 0.80 mmol, 60%). ^{1}H NMR (400 MHz, $CDCl_3$): δ = 8.17 (d, 2H, J=8.3 Hz, py H), 7.79 (d, 2H, J=7.8 Hz, py H), 4.65, 4.58 (AB q, 4H, J=13.7 Hz, -CH_2-), ≈3.5 ppm (m, 20H, cr); ^{13}C{^{1}H} NMR (100 MHz, $CDCl_3$): δ = 155.6 (py), 138.3 (py), 137.8 (py), 131.2 (py), 128.2 (py), 116.9 (CN), 70.7 (cr), 70.7 (cr), 70.6 (cr), 70.3 (cr), 70.0 (cr), 69.1 ppm (cr); HR CI-MS: m/z: calcd for $C_{24}N_4H_{29}O_6$: 469.208710; found: 469.207703 $[M+H]^+$ (deviation: 2.1 ppm); elemental analysis calcd (%) for $C_{24}H_{28}N_4O_6$: C 61.5, H 6.0, N 11.9; found: C 60.6, H 6.7, N 11.7.

6,6′-Bis(thiocarboxyamide)-3,3′-([18]crown-6)-2,2′-bipyridine: The dicarbonitrile (0.50 g, 1.07 mmol) was dissolved in a mixture of ethanol (20 mL) and triethylamine (1.5 mL). The solution was purged with $H_2S_{(g)}$ until it turned bright yellow and then the flask was stoppered and left overnight. The solvent was evaporated leaving a red/brown residue. This was purified using column chromatography (10% MeOH in CH_2Cl_2, silica gel) to give the title compound as a fine yellow powder (0.56 g, 98%). ^{1}H NMR (400 MHz, $CDCl_3$): δ = 9.35 (d, 2H, J=5.4 Hz, -NH_2), 8.70 (d, 2H, J=8.3 Hz, py H), 8.27 (d, 2H, J=5.4 Hz, -NH_2), 8.09 (d, 2H, J=8.3 Hz, py H), 4.51, 4.47 (AB q, 4H, J=13.2 Hz, -CH_2-), ≈3.5 ppm (m, 20H, cr); ^{13}C{^{1}H} NMR (100 MHz, $CDCl_3$): δ = 195.1 ($CSNH_2$), 152.9 (py), 148.6 (py), 138.2 (py), 136.6 (py), 124.9 (py), 70.7 (cr), 70.5 (cr), 70.4 (cr), 70.3 (cr), 70.0 (cr), 69.4 ppm (cr); ESI-MS: m/z: 537.1 $[M+H^+]$; elemental analysis calcd (%) for $C_{24}H_{32}N_4O_6S_2$: C 53.7, H 6.0, N 10.4; found: C 54.6, H 5.6, N 10.6.

6,6′-Bis(4-methylthiazol-2-yl)-3,3′-([18]crown-6)-2,2′-bipyridine (L^1): The dithio-carboxyamide (0.2 g, 0.37 mmol) and excess chloroacetone (ca. 3 mL) were heated at reflux for 8 h in ethanol (20 mL). After this time the solvent was removed and the resulting white residue was dissolved in water (15 mL), neutralised with $NaHCO_3$ and extracted into CH_2Cl_2 (3× 30 mL). The solvent was evaporated and the crude oil obtained was then purified by column chromatography (10% MeOH in CH_2Cl_2, silica gel) to give $\mathbf{L^1}$ as a pale oil (0.19 g, 0.31 mmol, 83%). Slow evaporation of an acetonitrile solution of $\mathbf{L^1}$ gave colourless crystals suitable for X-ray crystallographic analysis (see Supporting Information). ^{1}H NMR (400 MHz, $CDCl_3$): δ = 8.20 (d, 2H, J=8.3 Hz, py H^5), 8.09 (d, 2H, J=8.3 Hz, py H^4), 6.97 (s, 2H, tz H^5), 4.82 (s, 4H, -CH_2-), ≈3.5 (m, 20H, cr), 2.53 ppm (s, 6H, -CH_3); ^{1}H NMR (400 MHz, CD_3CN): δ = 8.18 (d, 2H, J=7.8 Hz, py H^5), 8.13 (d, 2H, J=7.8 Hz, py H^4), 7.15 (s, 2H, tz H^5), 4.72, 4.51 (AB q, 4H, J=12.7 Hz, -CH_2-), ≈3.5 (m, 20H, cr), 2.49 ppm (s, 6H, -CH_3); ^{13}C{^{1}H} NMR (100 MHz, $CDCl_3$): δ = 168.6 (th), 155.3 (py), 154.6 (py), 149.3 (py), 138.3 (py), 135.3 (py), 119.1 (th), 116.5 (th), 71.1 (cr), 71.0 (cr), 70.7 (cr), 70.6 (cr), 70.3 (cr), 66.3 (cr), 17.8 ppm (Me); ESI-MS: m/z: 613.4 $[M+H]^+$; elemental analysis calcd (%) for $C_{30}H_{36}N_4O_6S_2$: C 58.8, H 5.9, N 9.1; found: C 58.6, H 5.6, N 8.6.

Metal complexes: Crystalline samples were only obtained for those complexes in which the crown ether is occupied by a guest s-block cation. These samples were prepared by combining equimolar amounts (ca. 0.029 mmol) of $\mathbf{L^1}$ with an appropriate transition metal salt and an excess of s-block metal salt (typically 2–3 equivalents) in the minimum amount (5–10 mL) of solvent (MeCN or $MeNO_2$). The suspensions were sonicated for 10 minutes, filtered and concentrated in vacuo (if necessary), followed by either slow evaporation or diffusion of diethyl ether vapour to give crystals suitable for X-ray structural analysis. The characterisation of (purely) transition metal based complexes—for which crystalline samples were not obtained—was carried out on solutions prepared in situ by combining equimolar $\mathbf{L^1}$ and transition metal salt in an appropriate solvent (CD_3CN, CD_3NO_2). **CAUTION**: perchlorate salts are potentially explosive and should be handled with appropriate care. Those complexes described below which were isolated as perchlorates were only prepared in small quantities (10–20 mg) and we did not encounter any problems with them.

Data for $[Zn(L^1)][ClO_4]_2$ (in situ): ^{1}H NMR (400 MHz, CD_3CN): δ = 8.55 (d, 2H, J=7.9 Hz, py H^4), 8.28 (d, 2H, J=8.2 Hz, py H^5), 7.66 (s, 2H, tz H^5), 4.84 (s, 4H, -CH_2-), ≈3.5 (m, 20H, cr), 2.78 ppm (s, 6H, -CH_3); ESI-MS: m/z: 338.1 $[Zn(\mathbf{L^1})]^{2+}$, 777.1 $[Zn(\mathbf{L^1})(ClO_4)_2]^+$, 1389.3 $[Zn(\mathbf{L^1})_2(ClO_4)]^+$, 1653.2 $[Zn_2(\mathbf{L^1})_2(ClO_4)_3]^+$; HR ESI-MS: m/z: calcd for $C_{30}N_4S_2ZnO_6H_{36}$: 338.0678379; found: 338.0677810 $[Zn(\mathbf{L^1})]^{2+}$ (deviation: 0.2 ppm); calcd for $C_{60}N_8S_4Zn_2O_{24}H_{72}Cl_3$: 1649.1185308; found: 1649.1200540 $[Zn_2(\mathbf{L^1})_2(ClO_4)_3]^+$ (deviation: 1.0 ppm).

Data for $[Zn(L^1)(H_2O)_2\{Ba(ClO_4)_2(H_2O)_{0.75}\}][ClO_4]_2\cdot MeCN\cdot 0.5\,Et_2O$ ($\mathbf{1\cdot MeCN\cdot 0.5\,Et_2O}$): ^{1}H NMR (400 MHz, CD_3CN): δ = 8.47 (d, 2H, J=8.0 Hz, py H^4), 8.31 (d, 2H, J=8.1 Hz, py H^5), 7.64 (s, 2H, tz H^5), 5.19, 4.94 (AB q, 4H, J=13.0 Hz, -CH_2-), ≈3.5 (m, 20H, cr), 2.77 ppm (s, 6H, -CH_3); ESI-MS: as for above but instead of the double-stranded species $[Zn_2(\mathbf{L^1})_2(ClO_4)_3]^+$ a peak at m/z 1112 {$[Zn(\mathbf{L^1})Ba(ClO_4)_3]^+$} is observed.

Data for $[Cd(L^1)][ClO_4]_2$ and $[Cd_2(L^1)_2][ClO_4]_4$ (in situ): ^{1}H NMR (400 MHz, CD_3CN): δ = 8.50 (d, 2H, J=7.8 Hz, py H^4, SSM[6]; SSM = single-stranded mononuclear), 8.26 (d, 2H, J=8.3 Hz, py H^5, SSM), 7.88 (d, 2H, J=8.3, py H^4, DSD[7]; DSD = double-stranded dinuclear), 7.82 (d, 2H, J=8.3 Hz, py H^5, DSD), 7.66 (s, 2H, tz H^5, DSD), 7.65 (s, 2H, tz H^5, SSM), 4.83, 4.72 (AB q, 4H, J=13.7 Hz, -CH_2-, SSM), 4.57, 4.53 (AB q, 4H, J=13.5 Hz, -CH_2-, DSD), ≈3.5 (m, cr, SSM and DSD), 2.73 (s, 6H, -CH_3, SSM), 2.50 ppm (s, 6H, -CH_3, DSD); ESI-MS: m/z: 363.1 $[Cd(\mathbf{L^1})]^{2+}$, 669.2 $[Cd(\mathbf{L^1})_2]^{2+}$, 825.1 $[Cd(\mathbf{L^1})(ClO_4)]^+$, 1138.5 $[Cd_2(\mathbf{L^1})(ClO_4)_3]^+$, 1473.3 $[Cd(\mathbf{L^1})_2(ClO_4)]^+$, 1747.1 $[Cd_2(\mathbf{L^1})_2(ClO_4)_3]^+$.

Data for $[Cd(L^1)(ClO_4)_2\{Ba(ClO_4)_2\}]$ (2): ^{1}H NMR (400 MHz, CD_3CN): δ = 8.45 (d, 2H, J=8.0 Hz, py H^4), 8.32 (d, 2H, J=8.1 Hz, py H^5), 7.67 (s, 2H, tz H^5), 5.19, 5.92 (AB q, 4H, J=13.7 Hz, -CH_2-), ≈3.5 (m, 20H, cr), 2.73 ppm (s, 6H, -CH_3); ESI-MS: as for above but instead of the

[6] SSM = single-stranded mononuclear complex.
[7] DSD = double-stranded dinuclear complex.

double-stranded species $[Cd_2(\mathbf{L^1})_2(ClO_4)_3]^+$ only a peak at *m/z* 1160.4 $\{[Cd(\mathbf{L^1})Ba(ClO_4)_3]^+\}$ is observed.

Data for $[Hg_2(L^1)_2][ClO_4]_4$ (in situ): ^{1}H NMR (400 MHz, CD_3CN): δ = 8.12 (d, 2H, J = 8.1 Hz, py H^5), 7.97 (d, 2H, J = 8.2 Hz, py H^4), 7.90 (d, 2H, J = 1.1 Hz, tz H^5), 4.58, 4.29 (AB q, 4H, J = 13.7 Hz, -CH_2-), ≈3.5 (m, 20H, cr), 2.61 ppm (d, 6H, J = 1.1 Hz, -CH_3); ESI-MS: *m/z*: 407.1 $[Hg(\mathbf{L^1})]^{2+}$ and $[Hg_2(\mathbf{L^1})_2]^{4+}$, 713.2 $[Hg(\mathbf{L^1})_2]^{2+}$, 913.1 $[Hg(\mathbf{L^1})(ClO_4)]^+$ and $[Hg_2(\mathbf{L^1})_2(ClO_4)_2]^{2+}$, 1525.3 $[Hg(\mathbf{L^1})_2(ClO_4)]^+$, 1732.5 $[Hg_2(\mathbf{L^1})_2(Cl)_3]^+$ and 1925.2 $[Hg_2(\mathbf{L^1})_2(ClO_4)_3]^+$; HR ESI-MS: *m/z*: for $C_{60}N_8S_4Hg_2O_{24}H_{72}Cl_3$: calcd 1925.2014896; found: 1925.1938180 $[Hg_2(\mathbf{L^1})_2(ClO_4)_3]^+$ (deviation: 4.0 ppm).

Data for $[Hg_2(L^1)_2\{Na(ClO_4)(MeCN)\}\{Na\}][ClO_4]_5$·3 MeCN (3·3 MeCN): ^{1}H NMR (400 MHz, CD_3CN): δ = 8.19 (d, 2H, J = 8.1 Hz, py H^5), 7.99 (d, 2H, J = 8.2 Hz, py H^4), 7.95 (s, 2H, tz H^5), 4.42, 4.49 (AB q, 4H, J = 13.5 Hz, -CH_2-), ≈3.5 (m, 20H, cr), 2.62 ppm (s, 6H, -CH_3); ESI-MS: as for above but with additional peaks at *m/z* 2046.6 $[Hg_2(\mathbf{L^1})_2Na(ClO_4)_4]^+$ and 2170.1 $\{Hg_2(\mathbf{L^1})_2Na_2(ClO_4)_5]^+$.

Data for $[Hg(L^1)(ClO_4)_2\{Sr(ClO_4)_2\}]$·MeCN (4·MeCN): ^{1}H NMR (400 MHz, CD_3CN): δ = 8.45 (d, 2H, J = 8.2 Hz, py H^4), 8.35 (d, 2H, J = 8.2 Hz, py H^5), 7.95 (d, 2H, J = 1.1 Hz, tz H^5), 5.23, 4.94 (AB q, 4H, J = 13.5 Hz, -CH_2-), ≈3.5 (m, 20H, cr), 2.70 (d, 6H, J = 1.1 Hz, -CH_3); ESI-MS: *m/z*: 549.7 $[Hg(\mathbf{L^1})Sr(ClO_4)_2]^{2+}$, 570.5 $[Hg(\mathbf{L^1})(MeCN)Sr(ClO_4)_2]^{2+}$, 1198.5 $[Hg(\mathbf{1})(MeCN)Sr(ClO_4)_3]^+$, 2496.2 $[Hg_2(\mathbf{L^1})_2Sr_2(ClO_4)_7]^+$.

Data for $[Hg(L^1)(ClO_4)_2\{Ba(ClO_4)_2\}]$ (5): ^{1}H NMR (400 MHz, CD_3CN): as for **4**; ESI-MS: *m/z*: 574.5 $[Hg(\mathbf{L^1})Ba(ClO_4)_2]^{2+}$, 1248.3 $[Hg(\mathbf{L^1})Ba(ClO_4)_3]^+$; elemental analysis calcd (%) for $C_{30}H_{36}Ba_1Cl_4Hg_1N_4O_{22}S_2$: C 26.72, H 2.69, N 4.15; found: C 26.88, H 2.36, N 4.01.

Data for $[Cu_2(L^1)_2][PF_6]_2$ (in situ): ^{1}H NMR (400 MHz, CD_3CN): δ = 7.79 (d, 2H, J = 8.1 Hz, py H^5), 7.64 (d, 2H, J = 8.2 Hz, py H^4), 7.53 (s, 2H, tz H^5), 4.13, 4.01 (AB q, 4H, J = 13.5 Hz, -CH_2-), ≈3.5 (m, 20H, cr), 2.31 ppm (s, 6H, -CH_3); ESI-MS: *m/z*: 675.0 $[Cu(\mathbf{L^1})]^+$, 1496.6 $[Cu_2(\mathbf{L^1})_2(PF_6)]^{2+}$.

Data for $[Cu_2(L^1)_2\{Na(ClO_4)_2\}\{Na(MeCN)\}][ClO_4]_2$·0.5 MeCN·0.5 $NaClO_4$ (6·0.5 MeCN·0.5 $NaClO_4$): ^{1}H NMR (400 MHz, CD_3CN): δ = 7.85 (d, 2H, J = 8.1 Hz, py H^5), 7.60 (s, 2H, tz H^5), 7.59 (d, 2H, J = 8.1, py H^4), 4.28, 4.02 (AB q, 4H, J = 13.9 Hz, -CH_2-), ≈ 3.5 (m, 20H, cr), 2.38 ppm (s, 6H, -CH_3); elemental analysis calcd (%) for $C_{60}H_{72}Na_2Cl_4Cu_2N_9O_{28}S_4$·0.5 MeCN·0.5 $NaClO_4$: C 39.4, H 4.0, N 6.9; found C 39.5, H 3.9, N 7.1.

Data for $[Cu_2(L^1)_2\{Ba(ClO_4)_2\}_2][ClO_4]_2$·2 MeCN·0.5 Et_2O (7·2 MeCN·0.5 Et_2O): ^{1}H NMR (400 MHz, CD_3CN): δ = 7.82 (d, 2H, J = 8.3, py H^5), 7.66 (s, 2H, tz H^5), 7.49 (d, 2H, J = 8.2, py H^4), 4.49, 4.31 (AB q, 4H, J = 12.6, -CH_2-), ≈3.5 (m, 20H, cr), 2.47 ppm (s, 6H, -CH_3); ESI-MS: *m/z*: 675.0 $[Cu(\mathbf{L^1})]^+$, 1450.7 $[Cu_2(\mathbf{L^1})_2(ClO_4)]^+$, 1788.3 $[Cu_2(\mathbf{L^1})_2Ba(ClO_4)_3]^+$; elemental analysis calcd (%) for $C_{60}H_{72}Ba_2Cl_6Cu_2N_8O_{36}S_4$·2 MeCN: C 33.33, H 3.41, N 6.07; found C 33.17, H 3.61, N 6.59.

CCDC-637058 (**2**), -637059 (**4**), -637060 (**6**) and -637061 ($\mathbf{L^1}$) contain the supplementary crystallographic data for this paper. These data can be obtained free of charge from The Cambridge Crystallographic Data Centre via www.ccdc.cam.ac.uk/data_request/cif.

Acknowledgements

We would like to thank the EPSRC and the Universities of Bristol and Huddersfield for financial support. We also thank Dr. Martin Murray and Dr. Paul Gates for their generous help in obtaining the NOE and electrospray-ionisation spectra, respectively.

[1] a) J.-M. Lehn, *Supramolecular Chemistry*, VCH, Weinheim, **1995**; b) J. W. Steed, J. L. Atwood, *Supramolecular Chemistry*, Wiley, Chichester, **2000**; c) E. C. Constable in *Comprehensive Supramolecular Chemistry, Vol. 9* (Ed.: J.-P. Sauvage), Elsevier, Oxford, **1996**, pp. 213; d) R. M. Yeh, A. V. Davis, K. N. Raymond in *Comprehensive Coordination Chemistry II, Vol. 7* (Eds.: J. A. McCleverty, T. J. Meyer), Elsevier, Oxford, **2004**, pp. 327; e) C. Piguet, G. Bernardinelli, G. Hopfgartner, *Chem. Rev.* **1997**, *97*, 2005; f) M. Albrecht, *Chem. Rev.* **2001**, *101*, 3457; g) M. Albrecht, *Angew. Chem.* **2005**, *117*, 6606; *Angew. Chem. Int. Ed.* **2005**, *44*, 6448; h) M. J. Hannon, L. J. Childs, *Supramol. Chem.* **2004**, *16*, 7; i) P. N. W. Baxter, J.-M. Lehn, J. Fischer, M.-T. Youinou, *Angew. Chem.* **1994**, *106*, 2432; *Angew. Chem. Int. Ed. Engl.* **1994**, *33*, 2284; j) G. S. Hanan, D. Volkmer, U. S. Schubert, J.-M. Lehn, G. Baum, D. Fenske, *Angew. Chem.* **1997**, *109*, 1929; *Angew. Chem. Int. Ed. Engl.* **1997**, *36*, 1842; k) J. C. Jeffery, P. L. Jones, K. L. V. Mann, E. Psillakis, J. A. McCleverty, M. D. Ward, C. M. White, *Chem. Commun.* **1997**, 175; l) A. M. Garcia, D. M. Bassani, J.-M. Lehn, G. Baum, D. Fenske, *Chem. Eur. J.* **1999**, *5*, 1234; m) P. N. W. Baxter, J.-M. Lehn, B. O. Kneisel, G. Baum, D. Fenske, *Chem. Eur. J.* **1999**, *5*, 113; n) V. Maurizot, M. Yoshizawa, M. Kawano, M. Fujita, *Dalton Trans.* **2006**, *23*, 2750; o) S. R. Seidel, P. J. Stang, *Acc. Chem. Res.* **2002**, *35*, 972.

[2] C. J. Baylies, L. P. Harding, J. C. Jeffery, T. Riis-Johannessen, C. R. Rice, *Angew. Chem.* **2004**, *116*, 4615; *Angew. Chem. Int. Ed.* **2004**, *43*, 4515.

[3] C. J. Baylies, L. P. Harding, J. C. Jeffery, T. Riis-Johannessen, C. R. Rice, Ryan Moon, M. Whitehead, *Angew. Chem.* **2005**, *117*, 7069; *Angew. Chem. Int. Ed.* **2005**, *44*, 6909.

[4] C. J. Baylies, J. C. Jeffery, T. A. Miller, R. Moon, T. Riis-Johannessen, C. R. Rice, *Chem. Commun.* **2005**, 4158.

[5] T. Riis-Johannessen, J. C. Jeffery, A. P. H. Robson, C. R. Rice, L. P. Harding, *Inorg. Chim. Acta* **2005**, *358*, 2781.

[6] J. Sandström, *Dynamic NMR Spectroscopy*, Academic Press, New York, **1982**.

[7] R. F. Carina, A. F. Williams, C. Piguet, *Helv. Chim. Acta* **1998**, *81*, 548.

[8] R. D. Shannon, *Acta Crystallogr. Sect. A* **1976**, *32*, 751.

[9] P. N. W. Baxter, J. A. Connor, W. B. Scheizer, J. D. Wallis, *J. Chem. Soc. Dalton Trans.* **1992**, 3015.

[10] a) C. J. Pedersen, *Angew. Chem.* **1988**, *100*, 1053; *Angew. Chem. Int. Ed. Engl.* **1988**, *27*, 1021; b) J. S. Bradshaw, R. M. Izatt, A. V. Bordunov, C. Y. Zhu, J. K. Hathaway, *Crown Ethers in Comprehensive Supramolecular Chemistry, Vol. 1* (Ed.: G. W. Gokel), Elsevier, Oxford, **1996**, pp. 35.

[11] V. W.-W. Yam, Y.-L. Pui, K.-K. Cheung, N. Zhu, *New J. Chem.* **2002**, *26*, 536.

[12] a) L. Kovbasyuk, R. Krämer, *Chem. Rev.* **2004**, *104*, 3161; b) Y. Kubo, Y. Ishii, *J. Nanosci. Nanotechnol.* **2006**, *6*, 1489; c) J. Rebek Jr., *Acc. Chem. Res.* **1984**, *17*, 258; d) M. Takeuchi, M. Ikeda, A. Sugasaki, S. Shinkai, *Acc. Chem. Res.* **2001**, *34*, 865.

[13] SMART Diffractometer Control Software, Bruker Analytical X-ray Instruments Inc., Madison, WI, **1998**.

[14] SAINT Integration Software, Siemens Analytical X-ray Instruments Inc., Madison, WI, **1998**.

[15] SHELXTL Program System, Vers. 5.1, Bruker Analytical X-ray Instruments Inc., Madison, WI, **1998**.

[16] G. M. Sheldrick, SADABS: A Program for Absorption Correction with the Siemens SMART System, University of Göttingen (Germany), **1996**.

[17] A. L. Spek, *Acta Crystallogr. Sect. A* **1990**, *46*, C34; A. L. Spek, PLATON—A Multipurpose Crystallographic Tool, Utrecht (The Netherlands), **2003**.

[18] GEMINI, Autoindexing Program for Twinned Crystals, Vers. 1.02, Release 5, **2000**.

[19] J. D. Dunitz, V. Schomaker, K. N. Trueblood, *J. Chem. Phys.* **1988**, *88-89*, 856.

[20] a) J. Rebeck Jr. , J. E. Trend, R. V. Wattley, S. Chakravorti, *J. Am. Chem. Soc.* **1979**, *101*, 4333; b) B.-Z. Shan, Q. Zhao, N. Goswami, D. M. Eichhorn, D. P. Rillema, *Coord. Chem. Rev.* **2001**, *211*, 117.

Received: February 13, 2007
Published online: April 12, 2007

